

THE FREE-EDGE SINGULARITY DOMINATED ZONE
IN A COPPER-TUNGSTEN BIMATERIAL

by

Adam D. Goodworth

**ARTHUR LAKES LIBRARY
COLORADO SCHOOL OF MINES
GOLDEN, CO 80401**

ProQuest Number: 10794818

All rights reserved

INFORMATION TO ALL USERS

The quality of this reproduction is dependent upon the quality of the copy submitted.

In the unlikely event that the author did not send a complete manuscript and there are missing pages, these will be noted. Also, if material had to be removed, a note will indicate the deletion.



ProQuest 10794818

Published by ProQuest LLC (2018). Copyright of the Dissertation is held by the Author.


All rights reserved.

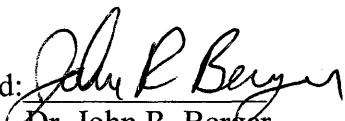
This work is protected against unauthorized copying under Title 17, United States Code
Microform Edition © ProQuest LLC.

ProQuest LLC.
789 East Eisenhower Parkway
P.O. Box 1346
Ann Arbor, MI 48106 – 1346

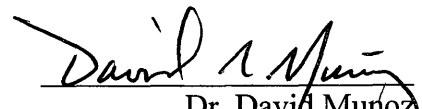
A thesis submitted to the Faculty and Board of Trustees of the Colorado School of Mines in partial fulfillment of the requirements for the degree of *Master of Science* (Engineering Systems).

Golden, Colorado
Date Nov. 17, 2004

Signed: 
Adam D. Goodworth

Approved: 
Dr. John R. Berger
Thesis Advisor

Golden, Colorado
Date 11/16/04


Dr. David Munoz
Department Head
Engineering

ABSTRACT

A bimaterial interface corner is studied with elasticity and boundary element data to derive the singularity dominated zone and the stress intensity factor. The analytical portion is solved using the Williams' approach, including the acquisition of five higher order terms (four of which are complex in nature). The boundary element data is derived from a Green's function formulation where the interface continuity conditions are satisfied analytically. Using a local collocation scheme, the stress intensity is determined using the higher order terms in the expansion of the radial stress equation. The nature of the singularity dominated zone is discussed and the two-term expansion zone is determined based on a 2 percent divergence from the 6-term model. Finally, the importance of the constant-stress term is described.

TABLE OF CONTENTS

SUBMITTAL PAGE.....	ii
ABSTRACT.....	iii
LIST OF FIGURES.....	vi
LIST OF TABLES.....	vii
ACKNOWLEDGEMENTS.....	viii
Chapter 1 INTRODUCTION.....	1
1.1 Importance Of Fracture Mechanic.....	1
1.2 Linear Elastic Fracture Mechanics.....	1
1.3 Functionally Graded Materials.....	3
1.4 Mechanics Of Bimaterials.....	4
1.5 The Singularity Dominated Zone.....	5
1.6 Overview Of The Thesis.....	5
Chapter 2 ELASTIC ANALYSIS FOR STRESSES AND DISPLACEMENTS.....	7
2.1 Introduction To Elastic Analysis.....	7
2.2 Stress And Displacement Calculation – Williams Approach.....	9
2.3 Eigenvalues.....	13
2.4 Analytical Solution.....	19
2.4.1 Real Eigenvalue (Not Equal To One).....	19
2.4.2 Eigenvalue Equal To One.....	22
2.4.3 Complex Eigenvalue.....	24
2.4.4 Analytical Solution Conclusion.....	32
Chapter 3 NUMERICAL ANALYSIS FOR STRESSES, DISPLACEMENTS, AND THE SINGULARITY DOMINATED ZONE.....	33
3.1 Introduction To Determining The Stress Intensity Factor.....	33
3.2 Boundary Element Method.....	35
3.3 Local Collocation.....	37
3.4 Singularly Dominated Zone.....	42

Chapter 4 RESULTS AND DISCUSSION.....	45
4.1 Collocation.....	45
4.1.1 Convergence Results.....	46
4.1.2 Accuracy Of Results.....	50
4.1.3 Stress Intensity Factor.....	55
4.2 Singularity Dominated Zone.....	57
4.3 Discussion And Future Research.....	62
Chapter 5 CONCLUSION.....	65
REFERENCES CITED.....	67
APPENDIX.....	75

LIST OF FIGURES

Figure 1.1: General Wedge Problem.....	2
Figure 2.1: The General Bimaterial Problem.....	7
Figure 2.2: Even Determinate Plot.....	16
Figure 2.3: Comparison Of Singular Powers.....	19
Figure 3.1: Schematic Of Boundary Element Model.....	37
Figure 3.2: The Singularity Dominated Zone (SDZ) Surrounding A Crack Tip.....	42
Figure 3.3: Internal Data Points In A Small Region.....	43
Figure 4.1: Convergence Of the First Two Leading Terms, C1 And C2.....	47
Figure 4.2: Convergence Of The Third And Fourth Terms, C3 And C4.....	48
Figure 4.3: Convergence Plot For C1 Through C4.....	49
Figure 4.4: Relative Error Vs. Number Of Parameters.....	51
Figure 4:5a-d: Model Comparisons For σ_{rr}	52
Figure 4:6: Singular Model Behavior.....	54
Figure 4:7: 2% Two Term Expansion Zone.....	59
Figure 4:8: 5% Two Term Expansion Zone.....	60
Figure 4:9: Two Term Expansion Zone.....	61

LIST OF TABLES

Table 2.1: First Six Positive Eigenvalues.....	18
Table 4.1: Local Collocation Values Of The Normalized Coefficients.....	50

ACKNOWLEDGEMENTS

I would like to acknowledge the support and contributions of Dr. John Berger, Dr. Paul Martin, and Dr. Ivar Reimanis. These three patiently reviewed my thesis and helped me through the “mountains” in the project. In addition, I’d like to acknowledge the assistance of Dr. Willy Hereman, Dr. Mark Lusk, and Keith Rozenburg. Finally, the support of my lovely wife, Anna, was crucial in the final lap.

CHAPTER 1

INTRODUCTION

1.1 Introduction To Fracture Mechanics

Materials frequently fail. For years, this was accepted as part of life with little accountability of preventative measures. However, in the 20th Century, as scientists began to understand failure mechanism better, predictive theories began to arise and verified experimentally. Most notable is the stress state criterion of failure. This states that a material will fail in brittle fracture within a region of discontinuity (crack, interface, notch, etc.) if the stress in this region reaches a critical value (1). The stress state failure criterion is the foundation of this thesis.

1.2 Linear Elastic Fracture Mechanics

Fracture mechanics is a relatively young field of engineering. Historically, the first attempt to analyze a crack problem was done in 1913 by C. E. Inglis (2). Inglis solved the problem of an elliptical hole in a plate under tension using the theory of elasticity. The energy associated with material fracture was first investigated by A. A. Griffith in 1921 (3), then further developed by Irwin in 1952. Irwin and Kies examined at how energy was released during crack growth in order to predict a material's resistance to crack propagation (4). However, a complete evaluation of fracture was not generally available until the development of linear elastic fracture mechanics (LEFM). One key contribution in the development of LEFM was the series of papers by M. L. Williams dealing with the stress and displacement fields near the apex of a wedge (5, 6). In 1952, Williams first solved the general wedge problem as shown in Figure 1.1. This analysis

was performed for an arbitrary apex angle. However, in 1957, Williams solved the limiting case where the internal angle approached 360 degrees. This wedge problem mathematically represents a crack.

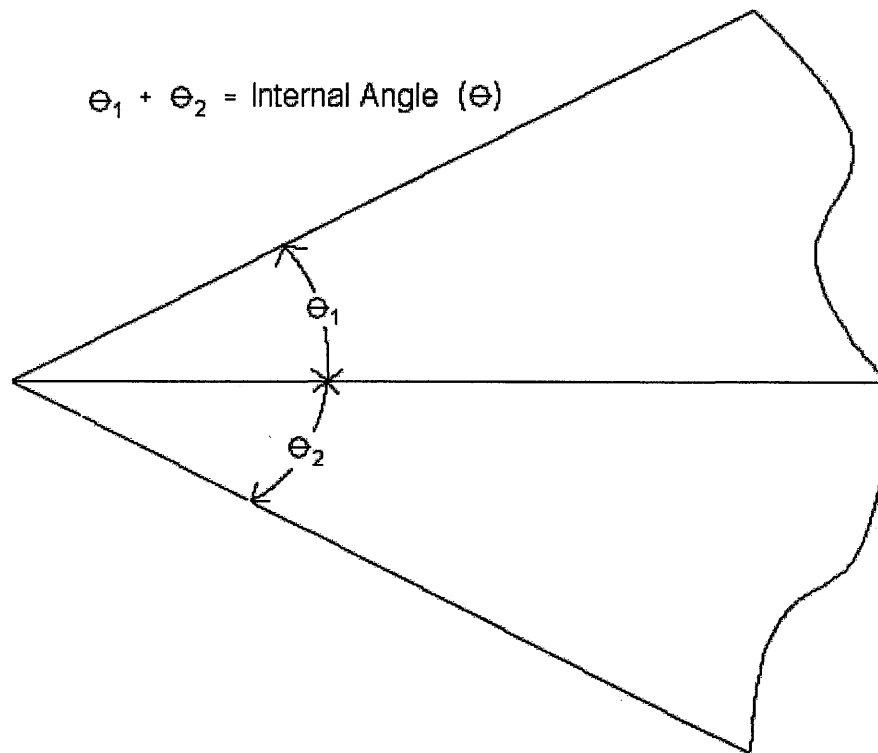


Figure 1.1: General Wedge Problem.

Williams' solution for the stresses at the tip of a crack in a linear elastic material was found to have an inverse square root dependence on the radial distance from the crack tip. The intensity of this stress singularity forms the basis for the stress-field approach to fracture used in LEFM. Williams' solutions for the stresses around a crack tip (as well as the strains and displacements) are obtained in series form. However, as the crack tip is

approached all terms except for the leading singular term vanish. Therefore, in the near field of the crack tip, it is the singular term which dominates the stress field.

The LEFM approach to fracture simply states that when the coefficient of the singular term reaches a critical value the crack will extend. The coefficient of the singular term is known as the stress intensity factor, and the critical value is known as the fracture toughness of the material. This simple growth law follows directly from the analysis of Irwin (4).

1.3 Functionally Graded Materials

Engineers are continually designing to optimize the performance of materials. Due to advances in processing techniques, materials with varying spatial composition can now be effectively produced. These functionally graded materials (FGMs) exhibit varying composition gradually or discretely throughout their thickness. When used strategically, FGMs can optimize performance in many practical materials, such as engine parts, structures, weldments, and armor (7). FGMs result in a stronger, more efficient use of materials than even before.

For FGMs to be used to their full potential both the application must be determined and the mechanism of failure must be found. Unfortunately, even where the application is well known, there are currently no established guidelines for selecting certain material combinations in functionally graded materials based on the failure mechanism.

Motivated by this, this thesis will describe the mechanics behind one particular aspect of FGM failure in a discrete, layered configuration. Here, we focus on the singular stress field found at the intersection of an interface and a free edge in a layered material.

1.4 Mechanics of Bimaterials

The mechanics of bimaterials has been studied extensively. While many researchers have made important contributions, for brevity, only a few that were used to aid this research will be discussed here. In 1968, Bogy considered two isotropic elastic quarter-planes bonded together (8). Bogy showed that the stresses at the intersection of the interface with the free surface of the bimaterial were singular in a manner similar to a crack. His investigation into the nature of the eigenvalues needed for calculating the state of stress showed that these could be real or complex (9). A year later, Dundurs discussed Bogy's work and showed that only two dimensionless parameters are needed to find the eigenfunctions for an interface problem (10). In 1979, Dempsey and Sinclair's investigation of the solution to the biharmonic equation extended understanding for various eigenvalue cases (11).

The advent of robust computer simulations, such as finite element methods and boundary element methods, brought about practical solutions to problems where a rigorous solution was unobtainable. For example, in 1994, Ding and Kumosa used the finite element method and a finite element iterative method to determine the singular stress field of an adhesively bonded joint and investigated the plastic zone (12). In 1998, Labossiere, Dunn, and Cunningham used the path independent H -integral to calculate the mixed mode stress intensities in a glass/silicon interface (13). Then, in 2000 Reedy showed the validity of the stress function approach for a steel/epoxy and aluminum/epoxy (14). Finally, in 2002, Akisanya and Meng investigated the validity and limitations of using a stress intensity factor to determine failure by looking at experimental results for aluminum/epoxy/aluminum and brass/solder/brass joints (15)

1.5 The Singularity Dominated Zone

The region surrounding a crack tip, or an interface-free edge intersection, where the stresses are dominated by the singular term in the stress field expansion, is called the Singularity Dominated Zone (SDZ). As one moves away from the source of the singularity, eventually the higher-order terms contribute in a significant way to the stresses and can no longer be ignored. In crack problems, the stress intensity factor, K , completely describes the state of stress inside the SDZ. For free-edge problems, the free-edge stress intensity factor, K_f , completely describes the state of stress in the SDZ. Therefore, for either crack or free-edge problems, knowledge of the extent of the SDZ is essential for fracture analysis.

To obtain the size and shape of the SDZ, the singular stress solution must be compared to a full-field solution obtained either experimentally (photoelasticity, moiré, etc.) or numerically (finite or boundary element methods). By comparing the singular solution with the full-field solution, the size and shape of the SDZ can be determined. Few examples of this type of calculation can be found in the literature. The only known calculation of this type concerned the extent of the SDZ in chevron notched fracture specimens (16). In this study, the SDZ was determined based on a comparison of the singular field and full-field photoelastic data using 2% to 10% differences in the Cartesian stresses.

1.6 Overview of the Thesis

As discussed in the previous sections, a stress singularity exists where the interface of a bimaterial intersects the free surface. This stress singularity will influence the initiation and growth of a crack positioned near this singularity. The goal of this thesis is to determine the extent of the SDZ in a specific copper-tungsten composite currently being

used in fracture studies. Knowledge of the SDZ will then provide guidance as to whether the free-edge singularity is affecting the initiation and growth of a crack located near the free edge.

The overview of this thesis is as follows. In Chapter 2, the full details of the elastic analysis for the free-edge stresses are presented. The details of the eigenvalue problem are shown and numerical results given for the copper-tungsten composite. Furthermore, particular details are given for complex eigenvalues as well as the case of degenerate eigenvalues.

In Chapter 3, results of a boundary element analysis of the copper-tungsten bimaterial are presented, as well as some details concerning the particular boundary element code used here. Numerical results for the stress field near the free-edge singularity are given, and the details of the local collocation approach to determining the stress field parameters presented. The chapter concludes with some general comments on the numerical aspects of determining the SDZ.

Numerical results are presented in Chapter 4 for the SDZ in the copper-tungsten composite. Convergence plots are presented showing the results of the local collocation, and SDZ sizes based on several approaches are given. This chapter concludes with a discussion of the major points of the results and some suggestions for future research. Chapter 5 points out the most important conclusions that are drawn from the thesis.

CHAPTER 2

ELASTIC ANALYSIS FOR STRESSES AND DISPLACEMENTS

2.1 Introduction To Elastic Analysis

The problem of interest is a bimaterial bonded together. The geometry is shown in Figure 2.1 below. The materials are assumed to be isotropic and behave linear elastically. Out-of-plane strains are assumed to be zero yielding plane-strain conditions.

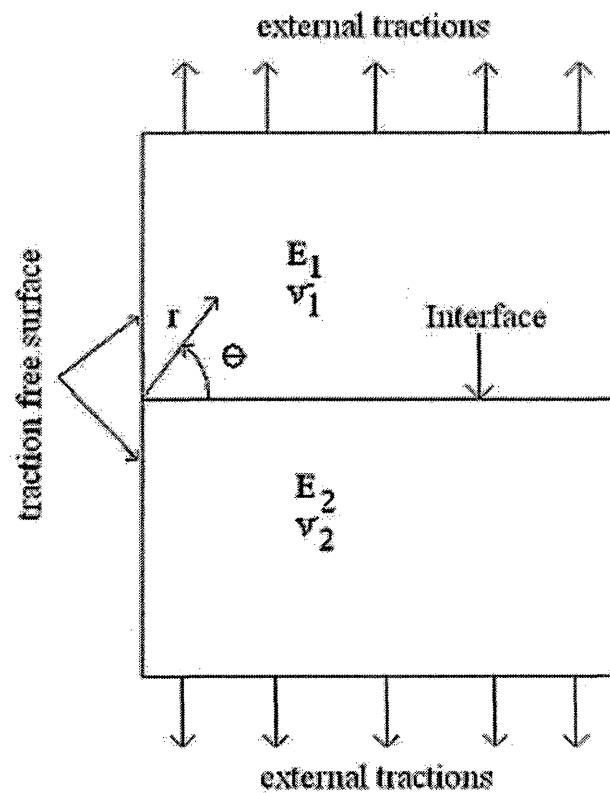


Figure 2.1: The General Bimaterial Problem.

The upper material has a modulus of elasticity is 160MPa with a Poisson's ratio of .330. The lower material has a modulus of elasticity of 190MPa with a Poisson's ratio of .286. This results in Dundur parameters of β equal to -.003395 and α equal to .070825. These values were obtained experimentally for an upper material composition of 80% Copper and 20% Tungsten and a lower material of 40% Copper and 60% Tungsten. Furthermore, the external tractions are 1000Pa.

There are several steps in finding the singularity dominated zone. First, the stresses and displacements are determined using either a Green's function or the Williams approach. Both of these approaches rely on a separation of variables solution method. In the case of the Green's function calculation, the displacement field is assumed to be a product of a radial term with an unknown function of θ . In the case of Williams' analysis, the Airy stress function is also assumed in a separated form, i.e.,

$$\phi = r^{\lambda+1} f(\theta) \quad (2.1)$$

The continuity conditions for displacement and traction across the interface, along with the boundary conditions, result in an eigenvalue problem. The eigenvalues (λ) are found through the solution of either an 8th order or 4th order polynomial depending on the analysis method chosen. Based on these eigenvalues, the unknown function $f(\theta)$, is found by solving the governing partial differential equation. The stress and displacement fields are now computed in both portions of the bimaterial. It should be noted that there is an infinite number of eigenvalues, so the resulting stress and displacement fields are written in series form summing over all eigenvalues. Each term in the series contains constants, which must be determined from the far-field loading.

Next, a boundary element method (BEM) program is used to find stress and displacement values near the free-edge singularity zone. With this data, a linear least-square fit is performed on the analytical stress and displacement fields in order to approximate the unknown constants appearing in these expressions. A convergence plot of the coefficient of the leading singular term versus the total number of terms used in the series is used to verify the leading term value. Finally, given the leading term, a singular parameter model (one-term expansion) is produced and the SDZ is found by comparing the singular term model to a twenty-term expansion. Similarly, the 2-parameter zone is found comparing the 2-term expansion to the twenty-term expansion. The twenty-term expansion is assumed to approximate the full-field solution. The SDZ is defined in this thesis as the zone where the difference in these calculations is 2%.

2.2 Stress And Displacement Calculations – Williams Approach

In finding the stresses and displacements, two techniques are implemented. The first method is the Williams approach based on an Airy stress function and the second approach is using a Green's function. In both cases, a general λ is assumed (no value was assigned to λ). Both results satisfy the equilibrium and constitutive requirements. Furthermore, when the boundary conditions and displacement continuities are enforced to solve the eigenvalue problem, both methods yield identical results for the leading eigenvalue. However, due to the simplicity of the Williams approach, the stresses and displacements in this thesis are found using this method.

The Williams approach of determining stresses and displacements is based on linear elasticity theory. Because of this, several steps must be taken to ensure a correct solution. Namely, continuity, equilibrium, and constitutive relationships must be satisfied.

We begin with the Airy Stress Function of the form given in eq. (2.1), where $f(\theta)$ is determined from the biharmonic equation solution which ensures compatibility. In polar coordinates, the biharmonic equation is

$$\nabla^4 \phi = \left(\frac{\partial^2}{\partial r^2} + \frac{1}{r} \frac{\partial}{\partial r} + \frac{1}{r^2} \frac{\partial^2}{\partial \theta^2} \right) \cdot \left(\frac{\partial^2}{\partial r^2} + \frac{1}{r} \frac{\partial}{\partial r} + \frac{1}{r^2} \frac{\partial^2}{\partial \theta^2} \right) \phi = 0 \quad (2.2)$$

Substituting eq. (2.1) in (2.2) yields an ordinary differential equation for $f(\theta)$,

$$\left(\frac{d^2}{d\theta^2} + (\lambda - 1)^2 \right) \cdot \left(\frac{d^2}{d\theta^2} + (\lambda + 1)^2 \right) f(\theta) = 0 \quad (2.3)$$

A general solution of equation (2.3) for $f(\theta)$ is

$$f(\theta) = A \sin((\lambda + 1)\theta) + B \cos((\lambda + 1)\theta) + C \sin((\lambda - 1)\theta) + D \cos((\lambda - 1)\theta) \quad (2.4)$$

The stresses can now be computed from the definition of the stresses in terms of the Airy stress function.

$$\sigma_{rr} = \frac{1}{r^2} \frac{\partial^2 \phi}{\partial \theta^2} + \frac{1}{r} \frac{\partial \phi}{\partial r} \quad (2.5)$$

$$\sigma_{\theta\theta} = \frac{\partial^2 \phi}{\partial r^2} \quad (2.6)$$

$$\sigma_{r\theta} = -\frac{\partial}{\partial r} \left(\frac{\partial \phi}{r \partial \theta} \right) \quad (2.7)$$

Substituting equations (2.1) and (2.4) in equations (2.5)-(2.7) yields the polar stresses

$$\sigma_{rr} = r^{\lambda-1} [A(-\lambda-1)\lambda \sin((\lambda+1)\theta) + B(-\lambda-1)\lambda \cos((\lambda+1)\theta) + C(-\lambda+3)\lambda \sin((\lambda-1)\theta) + D(-\lambda+3)\lambda \cos((\lambda-1)\theta)] \quad (2.8)$$

$$\sigma_{\theta\theta} = r^{\lambda-1} [A(\lambda+1)\lambda \sin((\lambda+1)\theta) + B(\lambda+1)\lambda \cos((\lambda+1)\theta) + C(\lambda+1)\lambda \sin((\lambda-1)\theta) + D(\lambda+1)\lambda \cos((\lambda-1)\theta)] \quad (2.9)$$

$$\sigma_{r\theta} = r^{\lambda-1} [A(-\lambda-1)\lambda \cos((\lambda+1)\theta) + B(\lambda+1)\lambda \sin((\lambda+1)\theta) + C(-\lambda+1)\lambda \cos((\lambda-1)\theta) + D(\lambda-1)\lambda \sin((\lambda-1)\theta)] \quad (2.10)$$

Now that the polar stresses have been formed, the strains are calculated by Hooke's Law,

$$\varepsilon_{rr} = \frac{1}{E} (\sigma_{rr} - \nu \sigma_{\theta\theta}) \quad (2.11)$$

$$\varepsilon_{\theta\theta} = \frac{1}{E} (\sigma_{\theta\theta} - \nu \sigma_{rr}) \quad (2.12)$$

$$\varepsilon_{r\theta} = \frac{1}{G} \sigma_{r\theta} \quad (2.13)$$

where E is the modulus of elasticity, ν is the Poisson's ratio, and G is the shear modulus defined as

$$G = \frac{E}{2(1+\nu)} \quad (2.14)$$

To use eqs. (2.11)-(2.13) in plane strain conditions, an effective modulus and Poisson's ratio are defined as

$$E' = \frac{E}{1-\nu^2} \quad (2.15)$$

$$\nu' = \frac{\nu}{1-\nu} \quad (2.16)$$

The displacements are calculated knowing the strains through the strain displacement equations,

$$\varepsilon_{rr} = \frac{\partial u}{\partial r} \quad (2.17)$$

$$\varepsilon_{\theta\theta} = \frac{1}{r} \frac{\partial v}{\partial \theta} + \frac{u}{r} \quad (2.18)$$

$$\gamma_{r\theta} = \frac{1}{r} \frac{\partial u}{\partial \theta} + \frac{\partial v}{\partial r} - \frac{v}{r} \quad (2.19)$$

where u and v are the radial and angular displacements, respectively. Integrating and solving for the displacements yields

$$\begin{aligned}
u = \int \varepsilon_{rr} dr = \frac{r^\lambda (1-\nu^2)}{E(-1+\nu)} & [A(\sin((\lambda+1)\theta) + \lambda \sin((\lambda+1)\theta)) + \\
& B(\cos((\lambda+1)\theta) + \lambda \cos((\lambda+1)\theta)) + C(-3\sin((\lambda-1)\theta) + \\
& 4\nu \sin((\lambda-1)\theta) + \lambda \sin((\lambda-1)\theta)) + D(-3\cos((\lambda-1)\theta) + \\
& 4\nu \cos((\lambda-1)\theta))] + g_1(\theta) \tag{2.20}
\end{aligned}$$

$$\begin{aligned}
v = \int (r \varepsilon_{\theta\theta} - u) d\theta = \frac{r^\lambda (1+\nu)}{E} & [A((1+\nu)(-\lambda-1)\cos((\lambda+1)\theta)) + \\
& B(\sin((\lambda+1)\theta) + \lambda \sin((\lambda+1)\theta)) + C((1+\nu)(-3+4\nu-\lambda)\cos((\lambda-1)\theta)) + \\
& D(3\sin((\lambda-1)\theta) - 4\nu \sin((\lambda-1)\theta) + \lambda \sin((\lambda-1)\theta))] + \int g_1(\theta) d\theta + g_2(r) \tag{2.21}
\end{aligned}$$

The functions $g_1(\theta)$ and $g_2(r)$ appearing in equations (2.20) and eq. (2.21) are equal to zero. This can be verified as follows. First, take the displacement field in equations (2.20) and (2.21) and recalculate the strains using equations (2.17)-(2.19). Next, calculate the shear strain directly from equations (2.10) and (2.13). Comparing the shear strain determined from the integrated displacements with the shear strain determined directly from the shear stress we see that $g_1(\theta)$ and $g_2(r)$ must be zero for the shear strain relations to agree.

2.3 Eigenvalues

For the analytical solution presented in the previous section to be valid, it must satisfy the boundary conditions on the free surfaces and conditions of displacement and traction continuity across the interface. For the geometry of interest shown in Figure 2.1, the external tractions are zero on the free-edge surface; therefore, the shear and hoop stresses must be zero along the free edge for both the upper and lower materials:

$$\begin{aligned}
\sigma_{r\theta}^1(r, \pi/2) &= 0 \\
\sigma_{\theta\theta}^1(r, \pi/2) &= 0 \\
\sigma_{r\theta}^2(r, -\pi/2) &= 0 \\
\sigma_{\theta\theta}^2(r, -\pi/2) &= 0
\end{aligned} \tag{2.22}$$

where the superscript represent the upper material (1) or the lower material (2). Across the interface, the displacements and tractions must be continuous,

$$\begin{aligned}
\sigma_{\theta\theta}^1(r, 0) &= \sigma_{\theta\theta}^2(r, 0) \\
\sigma_{r\theta}^1(r, 0) &= \sigma_{r\theta}^2(r, 0) \\
u^1(r, 0) &= u^2(r, 0) \\
v^1(r, 0) &= v^2(r, 0)
\end{aligned} \tag{2.23}$$

Substituting the stresses given by eqs. (2.8)-(2.10) and the displacements given by eqs. (2.20) and (2.21) in eqs. (2.22) and (2.23) yields the following linear system

$$\mathbf{A}(\lambda) \mathbf{x} = 0 \tag{2.24}$$

where

$$\mathbf{x} = \{A^1 \ B^1 \ C^1 \ D^1 \ A^2 \ B^2 \ C^2 \ D^2\}^T \tag{2.25}$$

and the 8x8 matrix $\mathbf{A}(\lambda)$ is formed from the stress and displacement expressions evaluated at the locations prescribed in equations (2.22) and (2.23). For the solution of eq. (2.24) to be nontrivial, the determinant of $\mathbf{A}(\lambda)$ must equal zero. The resulting eighth

order polynomial equation yields the eigenvalues, λ . However, the determinant equation derived by Martin (17) is used here.

Martin developed the Green's function for the problem shown in Figure 2.1. In elasticity, a Green's function gives a solution for the displacement field in a solid subjected to a point load. Green's functions play a critical role in boundary element methods (18) as will be discussed in Chapter 4 of this thesis. Here, our interest in the Green's function determined by Martin is focused on the polynomial obtained for the eigenvalue calculation that is simpler to that obtained by Williams, yet yields identical results.

Martin reduced the order of the determinant equation by applying the boundary conditions before forming the determinant; therefore, his matrix equation is less complex. Martin's analysis leads to a 4x4 linear system with the determinant of the matrix given by

$$\Delta(\lambda) = (\beta^2 - 1)S^4 + (1 + 2\lambda^2(\alpha - \beta)\beta)S^2 + \lambda^2(\lambda^2(\alpha - \beta)^2 - \alpha^2) \quad (2.26)$$

where $S = -\sin(\frac{1}{2}\pi\lambda)$, the Dundurs parameters (9) are

$$\begin{aligned} \beta &= \frac{\Gamma(k_1 - 1) - (k_2 - 1)}{\Gamma(k_1 + 1) + (k_2 + 1)} \\ \alpha &= \frac{\Gamma(k_1 + 1) - (k_2 + 1)}{\Gamma(k_1 + 1) + (k_2 + 1)} \end{aligned} \quad (2.27)$$

and Γ , k_1 and k_2 are defined as

$$\begin{aligned}\Gamma &= \frac{E_2(1+\nu_1)}{E_1(1+\nu_2)} \\ k_1 &= 3 - 4\nu_1 \\ k_2 &= 3 - 4\nu_2\end{aligned}\tag{2.28}$$

Further discussion of Dundurs parameters is outside the scope of this thesis, but they can be considered as measures of the degree of elastic mismatch in bimetals.

As stated, in general, there is an infinite number of eigenvalues that solve equation (2.26) and they can be real or complex in nature. Also, the solution of equation (2.26) is an even function of λ , as seen in Figure 2.2, where the determinant values are plotted along the vertical-axis and the lambda values are plotted along the horizontal-axis.

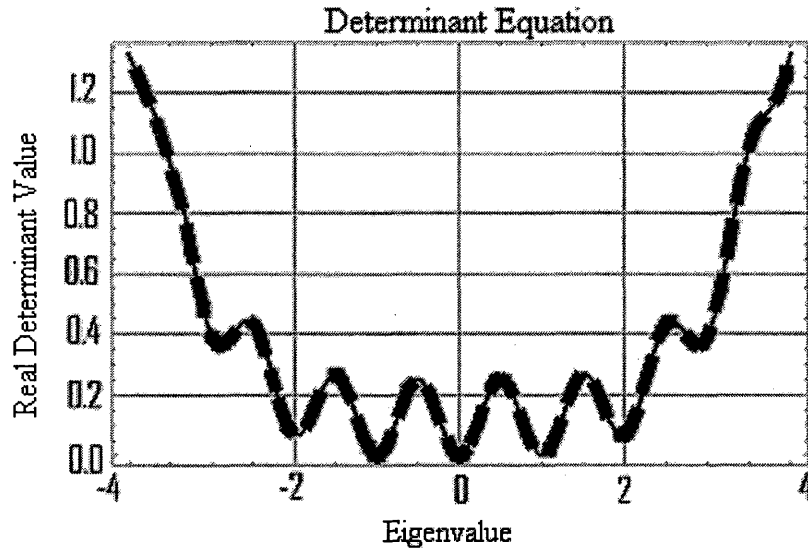


Figure 2.2: Even Determinant Plot

Of particular interest is when the determinant is equal to zero. The corresponding λ 's are called the eigenvalues. Most notably, the first positive root between zero and one is the

singular power eigenvalue, which determines the strength of the singularity. This can clearly be seen in equations (2.8)-(2.10) where the radial exponent is negative for $\lambda < 1$. Furthermore, we reject eigenvalues $\lambda < 0$ as they lead to unbounded displacements at the origin. Although the leading eigenvalue determines the strength of singular solution, six eigenvalues are obtained in order to develop the higher order expressions needed for analysis of the singularity dominated zone. To find the six eigenvalues accurately is not trivial. The first two roots are real and the subsequent roots are complex. Since the determinant equation for λ is transcendental, a numerical solution must be implemented to find the first two real solutions. However, our software used in this study, Mathematica 4.2, was unable to directly solve this type of equation. Therefore, a 40-term Taylor series expansion of the sine term in equation (2.26) was implemented to find the complex roots. A plot of the expansion series verses the actual determinant can be seen in Figure 2.2 above. The thick dashed line is the Taylor series and the thin, solid inside line is the actual determinant equation (2.26). It is clear that a 40-term Taylor expansion of the determinant is a reasonably accurate approximation for small roots.

For increased accuracy, an iterative routine is implemented to find the complex eigenvalues. After the first positive λ was found, $\lambda = \lambda_1$, the determinant is divided by $(1 - \lambda_1)$. After the second real root is found, $\lambda = \lambda_2$, the determinant was divided by $(1 - \lambda_1)(1 - \lambda_2)$. The complex roots obtained from this iterative process, using the Taylor series determinant, are then put into the original determinant equation from Martin to check the accuracy of this method. The results are shown below in Table 2.1.

Table 2.1: First Six Positive Eigenvalues

Eigenvalue	Determinant
0.995	6.66×10^{-16}
1.000	0.00
1.974 +/- .155 I	2.80×10^{-16}
2.942 +/- .326 I	9.04×10^{-16}
3.925 +/- .493 I	2.35×10^{-16}
4.920 +/- .631 I	1.18×10^{-12}

The results from this process are excellent for the first six positive roots. An eigenvalue of zero exists for this determinant; however, it is not permissible in the solution because a λ of zero results in unbounded strain energy computed on a closed contour around the tip of the wedge (1). Since the first positive root determines the strength of the singularity in the analytical model, it is of particular importance. The singular stress equation has the form $\sigma_{ij} = r^{\lambda-1} g_{ij}(\theta)$; thus, a λ between zero and one will cause the stress to approach infinity as the radius approaches zero. The value of this λ determines the intensity of the stress. For the problem of interest, the first root is $\lambda_1 = 0.995$. Comparing this to Williams crack problem, where the first root was determined to be $\lambda_1 = 0.500$, it is clear that our problem will not have a very strong singularity. This relationship is shown in Figure 2.3 on a log-log plot. The plot is a comparison of our copper-tungsten bimaterial singularity to Williams crack problem singularity.

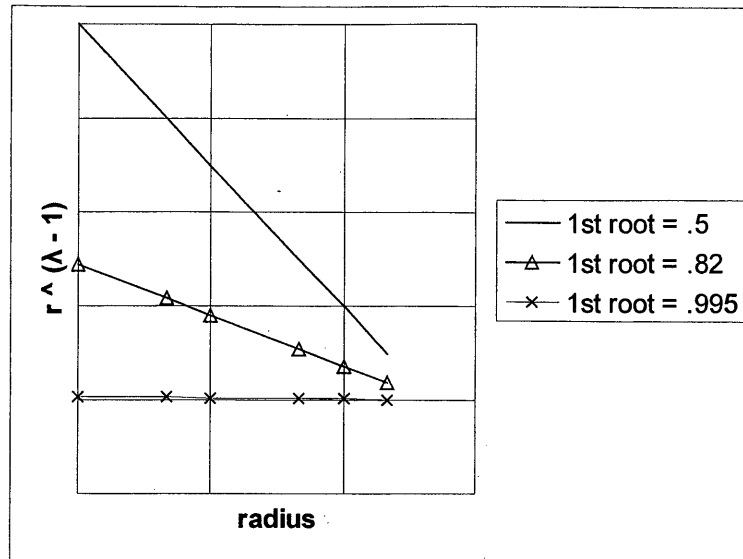


Figure 2.3: Comparison Of Singular Powers.

Finally, it is important to note that the complex λ 's occur as conjugate pairs. This must be the case in order to obtain real stresses and displacements as the eigenvalues are summed in the series expansion for higher order terms. The conjugate nature of the complex roots is discussed later in this thesis.

2.4 Analytical Solution

The stress and displacement equations are found by summing each model together for different values of λ . The formulation of stresses and displacements were shown in the previous section. However, that was for a general λ assumption. Now that we have obtained specific λ 's, we must recompute the stresses and displacements according to the steps taken in section 2.2.1. Starting with the Airy Stress function, we solve $f(\theta)$ for the different eigenvalue forms. There are three unique λ forms: λ real and not equal to one, λ

equal to one, and λ complex. When all these stress cases are summed, a full field solution is obtained. When using only the first λ case, the region of validity is the SDZ.

2.4.1 Real Eigenvalue (Not Equal To One)

The first case of λ is nearly identical to the formulation shown the previous section and will not be entirely repeated in this section. However, it is important to note several points. For the analytical solution, the assumed Airy stress function is

$$\phi = r^{\lambda+1} f(\psi) \quad (2.28)$$

where

$$f(\psi) = A \sin((\lambda + 1)\psi) + B \cos((\lambda + 1)\psi) + C \sin((\lambda - 1)\psi) + D \cos((\lambda - 1)\psi) \quad (2.29)$$

and ψ is defined as $\psi = \theta - \pi/2$. This definition makes applying boundary conditions on the free edge simple because ψ is equal to zero; and the sine terms in our stress equations drop out.

We solve the stresses using equations (2.5)-(2.7) and making the appropriate substitution of ψ . Then, we apply the boundary conditions, which must always be satisfied for the problem to make physical sense. Because of a traction free surface on the free-edge, when ψ is set to zero, the shear and hoop stress must also be zero,

$$\sigma_{\theta\theta}(r,0) = r^{\lambda-1}[B(\lambda + 1)\lambda + D(\lambda + 1)\lambda] = 0 \quad (2.30)$$

$$\sigma_{r\theta}(r,0) = r^{\lambda-1}[A(-\lambda - 1)\lambda + C(-\lambda + 1)\lambda] = 0 \quad (2.31)$$

It is clear that there must be a relationship between the constants to ensure the boundary conditions are satisfied. This relationship is

$$D = -B \quad (2.32)$$

$$C = -A \frac{(\lambda + 1)}{(\lambda - 1)} \quad (2.33)$$

After the boundary conditions are satisfied, the equilibrium and constitutive relationships are checked according to the description at the end of section 3.2. The result for the analytical solutions of λ being a real number, not equal to one is shown below:

$$\begin{aligned} \sigma_{rr} = \frac{2\lambda r^{\lambda-1}}{\lambda-1} & [\sin(\theta - \pi/2)(-A(2 - \lambda + \lambda^2)\cos(\lambda(\theta - \pi/2)) + \\ & B(\lambda - 1)^2 \sin(\lambda(\theta - \pi/2)) - \cos(\theta - \pi/2)(2B(\lambda - 1)\cos(\lambda(\theta - \pi/2)) + \\ & A(\lambda + 1)\sin(\lambda(\theta - \pi/2)))] \end{aligned} \quad (2.34)$$

$$\begin{aligned} \sigma_{\theta\theta} = \frac{2\lambda r^{\lambda-1}}{\lambda-1} & [A\lambda\cos(\lambda\theta - \pi/2)\sin(\theta - \pi/2) - (A\cos(\theta - \pi/2) + \\ & B(\lambda - 1)\sin(\theta - \pi/2))\sin(\lambda(\theta - \pi/2))] \end{aligned} \quad (2.35)$$

$$\begin{aligned} \sigma_{r\theta} = 2\lambda r^{\lambda-1} & [B\lambda\cos(\lambda(\theta - \pi/2))\sin(\theta - \pi/2) + (B\cos(\theta - \pi/2) + \\ & A(\lambda - 1)\sin(\theta - \pi/2))\sin(\lambda(\theta - \pi/2))] \end{aligned} \quad (2.36)$$

$$\begin{aligned} u = \frac{r^\lambda(1+\nu)}{E(-1+\lambda)} & (B(-1+\lambda)(-3+4\nu+\lambda)\cos((-1+\lambda)(\theta - \pi/2)) - \\ & (1+\lambda)(B(-1+\lambda)\cos((1+\lambda)(\theta - \pi/2)) + \\ & 2A((-2+2\nu+\lambda)\cos(\lambda(\theta - \pi/2))\sin(\theta - \pi/2) + \end{aligned}$$

$$(1 - 2\nu)\cos(\theta - \pi/2)\sin(\lambda(\theta - \pi/2)) \quad (2.37)$$

$$\begin{aligned} \nu = & \frac{1}{E(-1 + \lambda)} (Ar^\lambda(1 + \nu))((-1 + \lambda)(1 + \lambda)\cos((1 + \lambda)(\theta - \pi/2)) + \\ & (1 + \lambda)(3 - 4\nu + \lambda)\cos((\lambda - 1)(\theta - \pi/2))) + \\ & \frac{1}{E(-1 + \lambda)} (2Br^\lambda(1 + \nu)(-1 + \lambda)(-2 - 2\nu + \lambda)\cos(\lambda(\theta - \pi/2)) * \\ & \sin(\theta - \pi/2) + (1 - 2\nu)\cos(\theta - \pi/2)\sin(\lambda(\theta - \pi/2)) \end{aligned} \quad (2.38)$$

2.4.2 Eigenvalue Equal To One

When λ is equal one, solving the biharmonic equation yields a different solution than shown previously. The double root of $\lambda = 0$ in the differential equation yields a stress function of

$$f(\psi) = A\sin(2\psi) + B\cos(2\psi) + C\psi + D \quad (2.39)$$

where ψ is defined as $\theta - \pi/2$ and the $C\psi + D$ portion in $f(\psi)$ is the result of the double root. In this case, applying the boundary conditions, at ψ equal to zero, the hoop stress and shear stress are

$$\sigma_{\theta\theta}(r,0) = 2A + C = 0 \quad (2.40)$$

$$\sigma_{r\theta}(r,0) = D + B = 0 \quad (2.41)$$

Clearly, the resulting constant reduction relationship is

$$C = -2A \quad (2.42)$$

$$D = -B \quad (2.43)$$

This λ equals one case has some noteworthy attributes. The stresses are only a function of theta, independent of a radial component. This has the same form as the ‘T-stress’ in the crack problem (1). In the crack problem, the ‘T-stress’ is a uniform stress, parallel to the crack plane. For the bimaterial, the resulting stresses and displacements are shown below.

$$\sigma_{rr} = -2(B + 2A(\theta - \pi/2) + B \cos(2(\theta - \pi/2)) + A \sin(2(\theta - \pi/2))) \quad (2.44)$$

$$\sigma_{\theta\theta} = 2(-B - 2A(\theta - \pi/2) + B \cos(\theta - \pi/2) + A \sin(2(\theta - \pi/2))) \quad (2.45)$$

$$\sigma_{r\theta} = 4B \sin(\theta - \pi/2)(B \cos(\theta - \pi/2) + A \sin(\theta - \pi/2)) \quad (2.46)$$

$$u = \frac{2r(1+\nu)((-1+2\nu)(B+2A(\theta-\pi/2)) - B \cos(2(\theta-\pi/2)) - A \sin(2(\theta-\pi/2)))}{E} \quad (2.47)$$

$$v = \frac{-2r(1+\nu)(A\cos(2(\theta - \pi/2)) - B\sin(2(\theta - \pi/2)))}{E} + g_2(r) \quad (2.48)$$

Note that in the λ equals one case, $g_2(r)$ is included in the displacement equation and is not equal to zero. When checking equilibrium, following the process described in section 2.2, the shear strain (2.10) and (2.13) equilibrium is not satisfied. In this case, one function of integration, $g_2(r)$, in the displacement calculation is not zero. Detailed calculations of the displacements can be found in the appendix, the result for $g_2(r)$ is

$$g_2(r) = r \left(\frac{8B}{E} \log(r) + L \right) \quad (2.49)$$

where L is a constant of integration. This equation is bounded and tends to zero as the radius approaches zero. The stress and displacement results from this case are unique and play important role in our problem that will be evident in the remaining chapters.

2.4.3 Complex Eigenvalue

The complex case of λ is involved. It is important to remember that the stresses will be summed together. Since the complex eigenvalues come in conjugates of each other, the summation of these complex conjugate cases yield real stresses and displacements. Therefore, each stress and displacement formed from an eigenvalue must be a summation of one complex eigenvalue and its conjugate, defined as

$$\lambda = \zeta + i\eta \quad (2.50)$$

$$\bar{\lambda} = \zeta - i\eta \quad (2.51)$$

Now, the Airy stress function takes the form

$$\phi = r^{\lambda+1} f(\psi) + r^{\bar{\lambda}+1} \bar{f}(\psi) \quad (2.52)$$

where the $f(\psi)$ is defined as equation 2.29 and $\bar{f}(\psi)$ is defined as

$$\bar{f}(\psi) = \bar{A} \sin((\lambda+1)\psi) + \bar{B} \cos((\lambda+1)\psi) + \bar{C} \sin((\lambda-1)\psi) + \bar{D} \cos((\lambda-1)\psi) \quad (2.53)$$

The expression $r^{\lambda+1}$, with a complex λ defined as equation 2.50, is equal to $r^\zeta r^{i\eta}$.

Furthermore, the complex portion of this term has oscillatory behavior, as shown in equation 2.54 below.

$$r^{i\eta} = e^{i\eta \log(r)} = \cos(\eta \log(r)) + i \sin(\eta \log(r)) \quad (2.54)$$

The $f(\psi)$ and $\bar{f}(\bar{\psi})$ are also a function of complex terms, as shown in the redefinition of the unknown parameters below.

$$\begin{aligned} A &= A_1 + i A_2 \\ B &= B_1 + i B_2 \\ C &= C_1 + i C_2 \\ D &= D_1 + i D_2 \\ \bar{A} &= A_1 - i A_2 \\ \bar{B} &= B_1 - i B_2 \\ \bar{C} &= C_1 - i C_2 \\ \bar{D} &= D_1 - i D_2 \end{aligned} \quad (2.55)$$

The complex constants A , B , C , and D , and their conjugate pairs, are related as equation (2.32) and (2.33). Namely,

$$\begin{aligned}
D &= -B \\
C &= -A \frac{(\lambda + 1)}{(\lambda - 1)} \\
\bar{D} &= -\bar{B} \\
\bar{C} &= -\bar{A} \frac{(\bar{\lambda} + 1)}{(\bar{\lambda} - 1)}
\end{aligned} \tag{2.56}$$

Thus, the stress function is now in its complex form, where $\phi_1 = r^{\lambda+1} f(\psi)$ and $\phi_2 = r^{\bar{\lambda}+1} f(\bar{\psi})$ each contain imaginary components. However, for a given complex pair, the summation of the stress functions ϕ_1 and ϕ_2 results in a real stress function,

$$\begin{aligned}
\phi = \phi_1 + \phi_2 &= \frac{1}{\eta^2 + (\zeta - 1)^2} (4r^{\zeta+1} (\cosh[\eta\psi] ((A_1(\beta\eta + \alpha(\eta^2 + (\zeta - 1)\zeta)) + \\
&A_2(\alpha\eta - \beta(\eta^2 + (\zeta - 1)\zeta))) \cos[\zeta\psi] \sin[\psi] - ((A_1(\beta\eta + \alpha(\zeta - 1)\zeta)) + \\
&A_2(\beta + \alpha\eta - \beta\zeta)) \cos[\psi] + (B_2\alpha - B_2\beta)(\eta^2 + (\zeta - 1)^2) \sin[\psi]) \sin[\zeta\psi] + \\
&((A_2(\beta\eta + \alpha(\zeta - 1)) - A_1(\beta + \alpha\eta - \beta\zeta)) \cos[\psi] \cos[\zeta\psi] + \\
&\sin[\psi] ((B_2\alpha + B_1\beta)(\eta^2 + (\zeta - 1)^2) \cos[\zeta\psi] + (A_2(\beta\eta + \alpha(\eta^2 + (\zeta - 1)\zeta)) + \\
&A_1(-\alpha\eta + \beta(\eta^2 + (\zeta - 1)\zeta))) \sin[\zeta\psi]) \sinh[\eta\psi])
\end{aligned} \tag{2.57}$$

Further details of this derivation can be found in the appendix. For the stress function and the definitions above, the resulting stresses and displacements from the complex eigenvalues are as follows:

$$\begin{aligned}
\sigma_{rr} = & \frac{1}{\eta^2 + (-1 + \xi)^2} * \\
& (4r^{-1+\xi} (\cosh[\eta\psi] (\cos[\psi] (2(n^2 + (-1 + \xi)^2) \cos[\xi\psi]) * \\
& ((B_{2\eta} - B_{1\xi}) \cos[\eta \log[r]] + (B_{1\eta} + B_{2\xi}) \sin[\eta \log[r]]) + \\
& \sin[\xi\psi] ((A_2\eta(-1)\eta^2 - 2\xi + \xi^2) - A_1(\eta^2(2 + \xi) + \xi(-1 + \xi^2))) * \\
& \cos[\eta \log[r]] + (A_1\eta(-1 + \eta^2 - 2\xi + \xi^2) + \\
& A_2(\eta^2(2 + \xi) + \xi(-1 + \xi^2))) \sin[\eta \log[r]]) + \\
& \sin[\psi] ((\eta^2 + (-1 + \xi)^2) \sin[\xi\psi] ((B_2(\eta - 2\eta\xi) - B_1(\eta^2 + \xi - \xi^2)) * \\
& \cos[\eta \log[r]] + (B_1(\eta - 2\eta\xi) + B_2(\eta^2 + \xi - \xi^2)) \sin[\eta \log[r]]) + \\
& \cos[\xi\psi] ((2A_2\eta(1 + \xi + \eta^2\xi - 2\xi^2 + \xi^3) + \\
& A_1(\eta^4 + \eta^2(3 - 2\xi) + \xi(-2 + \xi + 2\xi^2 - \xi^3))) \cos[\eta \log[r]] + \\
& (2A_1\eta(1 + \xi + \eta^2\xi - 2\xi^2 + \xi^3) - A_2(\eta^4 + \eta^2(3 - 2\xi) + \\
& \xi(-2 + \xi + 2\xi^2 - \xi^3))) \sin[\eta \log[r]])) + \\
& (\cos[\psi] (-2(\eta^2 + (-1 + \xi)^2) \sin[\xi\psi] ((B_1\eta + B_2\xi) \cos[\eta \log[r]] + \\
& (-B_2\eta + B_1\xi) \sin[\eta \log[r]]) + \\
& \cos[\xi\psi] ((A_1\eta(-1 + \eta^2 - 2\xi + \xi^2) + A_2(\eta^2(2 + \xi) + \xi(-1 + \xi^2))) * \\
& \cos[\eta \log[r]] + (-A_2\eta(-1 + \eta^2 - 2\xi + \xi^2) + \\
& A_1(\eta^2(2 + \xi) + \xi(-1 + \xi^2))) \sin[\eta \log[r]] + \\
& \sin[\psi] ((\eta^2 + (-1 + \xi)^2) \cos[\xi\psi] ((B_1(\eta - 2\eta\xi) + B_2(\eta^2 + \xi - \xi^2)) * \\
& \cos[\eta \log[r]] + (B_2\eta(-1 + 2\xi) + B_1(\eta^2 + \xi - \xi^2)) \sin[\eta \log[r]]) + \\
& \sin[\xi\psi] ((-2A_1\eta(1 + \xi + \eta^2\xi - 2\xi^2 + \xi^3) + A_2 * \\
& (\eta^4 + \eta^2(3 - 2\xi) + \xi(-2 + \xi + 2\xi^2 - \xi^3))) \cos[\eta \log[r]] + \\
& (2A_2\eta(1 + \xi + \eta^2\xi - 2\xi^2 + \xi^3) + A_1(\eta^4 + \eta^2(3 - 2\xi) + \\
& \xi(-2 + \xi + 2\xi^2 - \xi^3))) \sin[\eta \log[r]])) \sinh[\eta\psi])
\end{aligned} \tag{2.58}$$

$$\begin{aligned}
\sigma_{\theta\theta} = & \frac{1}{\eta^2 + (-1 + \xi)^2} * \\
& (4r^{-1+\xi} (\cosh[\eta\psi] (\cos[\xi\psi] \sin[\psi] ((A_1(\eta^2 - \eta^4 + 4\eta^2\xi - \xi^2 + \xi^4) - \\
& 2A_2(\eta^2(1 + \xi) + \xi(-1 - \xi + \xi^2)))) \cos[\eta \log[r]] + \\
& (A_2(\eta^4 + \xi^2 - \xi^4 - \eta^2(1 + 4\xi)) - 2A_1\eta(\eta^2(1 + \xi) + \xi(-1 - \\
& \xi + \xi^2))) \sin[\eta \log[r]]) + \sin[\xi\psi] ((-\eta^2 - (-1 + \xi)^2) * \\
& \sin[\psi] ((-B_2(\eta - 2\eta\xi) + B_1(-\eta^2 + \xi + \xi^2)) \cos[\eta \log[r]] - \\
& (B_1(\eta + 2\eta\xi) + B_2(-\eta^2 + \xi + \xi^2)) \sin[\eta \log[r]]) + \\
& \cos[\psi] ((A_2\eta(-1 + \eta^2 - 2\xi + \xi^2) - A_1(\eta^2(2 + \xi) + \xi(-1 + \xi^2))) * \\
& \cos[\eta \log[r]] + (A_1\eta(-1 + \eta^2 - 2\xi + \xi^2) + \\
& A_2(\eta^2(2 + \xi) + \xi(-1 + \xi^2))) \sin[\eta \log[r]]) + \\
& (\cos[\psi] \cos[\xi\psi] ((A_1\eta(-1 + \eta^2 - 2\xi + \xi^2) + \\
& A_2(\eta^2(2 + \xi) + \xi(-1 + \xi^2))) \cos[\eta \log[r]] + \\
& (-AA_2\eta(-1 + \eta^2 - 2\xi + \xi^2) + A_1(\eta^2(2 + \xi) + \xi(-1 + \xi^2))) * \\
& \sin[\eta \log[r]]) - \sin[\psi] ((-\eta^2 - (-1 + \xi)^2) \cos[\xi\psi] * \\
& ((B_1(\eta + 2\eta\xi) - B_2(-\eta^2 + \xi + \xi^2)) \cos[\eta \log[r]] + \\
& (-B_2(\eta + 2\eta\xi) + B_1(-\eta^2 + \xi + \xi^2)) \sin[\eta \log[r]]) - \sin[\xi\psi] * \\
& ((A_2(\eta^2 - \eta^4 + 4\eta^2\xi - \xi^2 + \xi^4) + 2A_1\eta(\eta^2(1 + \xi) + \xi(-1 - \\
& \xi + \xi^2))) \cos[\eta \log[r]] + A_1(\eta^2 - \eta^4 + 4\eta^2\xi - \xi^2 + \xi^4) - 2A_2\eta * \\
& (\eta^2(1 + \xi) + \xi(-1 - \xi + \xi^2))) \sin[\eta \log[r]])) \sinh[\eta\psi])
\end{aligned} \tag{2.59}$$

$$\begin{aligned}
\sigma_{r,\theta} = & (4r^{-1+\xi} (\cosh[\eta\psi] (\cos[\xi\psi] \sin[\psi] ((2B_2(\eta^2 - \xi^2)) \cos[\eta \log[r]] + \\
& 2B_1\eta\xi + B_2(\eta^2 + \xi^2)) \sin[\eta \log[r]]) + \\
& \sin[\xi\psi] \cos[\psi] ((B_2\eta - B_1\xi) \cos[\eta \log[r]] + (B_1\eta + B_2\xi) \sin[\eta \log[r]]) + \\
& \sin[\psi] ((A_2(\eta + 2\eta\xi) + A_1(\eta^2 - \xi(1 + \xi))) \cos[\eta \log[r]] + \\
& (A_1(\eta + 2\eta\xi) + A_2(-\eta^2 + 2\xi + \xi^2)) \sin[\eta \log[r]])) + \\
& (\cos[\psi] \cos[\xi\psi] ((B_1\eta + B_2\xi) \cos[\eta \log[r]] + (B_2\eta + B_1\xi) \sin[\eta \log[r]]) + \\
& (\sin[\psi] \sin[\xi\psi] ((B_2\eta^2 - 2B_1\eta\xi - B_2\xi^2) \cos[\eta \log[r]] + \\
& (B_1\eta^2 - 2B_2\eta\xi - B_1\xi^2) \sin[\eta \log[r]] + \\
& \cos[\xi\psi] ((A_1(\eta + 2\eta\xi) + A_2(-\eta^2 + 2\xi + \xi^2)) \cos[\eta \log[r]] + \\
& (-A_2(\eta + 2\eta\xi) + A_1(-\eta^2 + 2\xi + \xi^2)) \sin[\eta \log[r]]))) \sinh[\eta\psi]) \quad (2.60)
\end{aligned}$$

$$\begin{aligned}
u = & \frac{1}{E(\eta^2 + (-1 + \xi)^2)} (4r^{-1+\xi}(1 + \nu))^* \\
& (\cosh[\eta\psi](\cos[\psi](2(-1 + \nu)(\eta^2 + (-1 + \xi)^2)\cos[\xi\psi](B_1\cos[\eta\log[r]] - \\
& B_2\sin[\eta\log[r]]) + (-1 + 2\nu)\sin[\xi\psi]((2A_2\eta + A_1(-1 + \eta^2 + \xi^2))^* \\
& \cos[\eta\log[r]]) + ((2A_1\eta - A_2(-1 + \eta^2 + \xi^2))\sin[\eta\log[r]])) - \\
& \sin[\psi](\eta^2 + (-1 + \xi)^2)\sin[\xi\psi]((B_2\eta - B_1(-1 + 2\nu + \xi))^* \\
& \cos[\eta\log[r]] + (B_1\eta + B_2(-1 + 2\nu + \xi))\sin[\eta\log[r]])) + \\
& \cos[\xi\psi]((-A_2\eta(3 - 4\nu + \eta^2 - 2\xi + \xi^2) + A_1(2 + (-1 + \eta^2)\xi - \\
& 2\xi^2 + \xi^3 + 2\nu(-1 + \eta^2 + \xi^2)))\cos[\eta\log[r]] - \\
& (A_1\eta(3 - 4\nu + \eta^2 - 2\xi + \xi^2) + A_2(2 + (-1 + \eta^2)\xi - \\
& 2\xi^2 + \xi^3 + 2\nu(-1 + \eta^2 + \xi^2)))\sin[\eta\log[r]])) - \\
& \cos[\psi](-2(-1 + \nu)(\eta^2 + (-1 + \xi)^2)\sin[\xi\psi]^* \\
& (B_2\cos[\eta\log[r]] + B_1\sin[\eta\log[r]])) + (-1 + 2\nu)^* \\
& \cos[\xi\psi]((-2A_1\eta - A_2(-1 + \eta^2 + \xi^2))\cos[\eta\log[r]]) + \\
& (2A_1\eta + A_1(-1 + \eta^2 + \xi^2))\sin[\eta\log[r]])) + \\
& \sin[\psi](\eta^2 + (-1 + \xi)^2)\cos[\xi\psi]((B_1\eta - B_2(-1 + 2\nu + \xi))^* \\
& \cos[\eta\log[r]] + (-B_2\eta + B_1(-1 + 2\nu + \xi))\sin[\eta\log[r]] + \\
& \sin[\xi\psi]((A_1\eta(3 - 4\nu + \eta^2 - 2\xi + \xi^2) + A_2(2 + (-1 + \eta^2)\xi - \\
& 2\xi^2 + \xi^3 + 2\nu(-1 + \eta^2 + \xi^2)))\cos[\eta\log[r]])) + \\
& (-A_2\eta(3 - 4\nu + \eta^2 - 2\xi + \xi^2) + A_1(2 + (-1 + \eta^2)\xi - 2\xi^2 + \\
& \xi^3 + 2\nu(-1 + \eta^2 + \xi^2)))\sin[\eta\log[r]]))\sinh[\eta\psi])
\end{aligned} \tag{2.61}$$

$$\begin{aligned}
v = & \frac{1}{E11(\eta^2 + (-1 + \xi)^2)} (4r^\xi(1 + \nu))^* \\
& (\cosh[\eta\psi](\cos[\psi](1 - 2\nu)(\eta^2 + (-1 + \xi)^2)\sin[\xi\psi](B_1\cos[\eta\log[r]] - \\
& B_2\sin[\eta\log[r]]) + 2(-1 + \nu)\cos[\xi\psi]((2A_2\eta + A_1(-1 + \eta^2 + \xi^2))^* \\
& \cos[\eta\log[r]]) + ((2A_1\eta - A_2(-1 + \eta^2 + \xi^2))\sin[\eta\log[r]]) + \\
& \sin[\psi]((\eta^2 + (-1 + \xi)^2)\cos[\xi\psi]((B_2\eta - B_1(-2 + 2\nu - \xi))^* \\
& \cos[\eta\log[r]] + (B_1\eta + B_2(2 - 2\nu + \xi))\sin[\eta\log[r]]) + \\
& \sin[\xi\psi]((A_2\eta(-3 + 4\nu + \eta^2 - 2\xi + \xi^2) + A_1(1 + \xi)(1 + \xi)^2 - \\
& \eta^2((3 + \xi) + 2\nu(-1 + \eta^2 + \xi^2)))\cos[\eta\log[r]] + \\
& (A_1\eta(-3 + 4\nu + \eta^2 - 2\xi + \xi^2) + A_2((-1 + \xi)(1 + \xi)^2 + \\
& \eta^2(3 + \xi) - 2\nu(-1 + \eta^2 + \xi^2)))\sin[\eta\log[r]])) + \\
& \cos[\psi](-1 + 2\nu)(\eta^2 + (-1 + \xi)^2)\cos[\xi\psi]^* \\
& (B_2\cos[\eta\log[r]] + B_1\sin[\eta\log[r]])) + 2(-1 + \nu)^* \\
& \sin[\xi\psi]((-2A_1\eta - A_2(-1 + \eta^2 + \xi^2))\cos[\eta\log[r]] + \\
& (2A_2\eta + A_1(-1 + \eta^2 + \xi^2))\sin[\eta\log[r]])) - \\
& \sin[\psi]((\eta^2 + (-1 + \xi)^2)\sin[\xi\psi]((B_1\eta + B_2(2 - 2\nu + \xi))^* \\
& \cos[\eta\log[r]] + (-B_2\eta + B_1(2 - 2\nu + \xi))\sin[\eta\log[r]]) + \\
& \cos[\xi\psi]((A_1\eta(-3 + 4\nu + \eta^2 - 2\xi + \xi^2) + \\
& A_2(-1 + \xi)(1 + \xi)^2 + \eta^2(3 + \xi) - 2\nu(-1 + \eta^2 + \xi^2)))^* \\
& \cos[\eta\log[r]] - (A_2\eta(-3 + 4\nu + \eta^2 - 2\xi + \xi^2) + \\
& A_1(1 - \xi)(1 + \xi)^2 - \eta^2(3 + \xi) + 2\nu(-1 + \eta^2 + \xi^2)))^* \\
& \sin[\eta\log[r]]))\sinh[\eta\phi])
\end{aligned} \tag{2.62}$$

where ψ is defined as $\theta - \pi/2$. The determination of $g_1(\theta)$ and $g_2(r)$ has been omitted due to irrelevancy. The displacement equations are not used in this thesis for determination of the singularity dominated zone. Furthermore, after the stress intensity factor is determined from the stresses, if displacements were to be examined inside the SDZ, only the first two real displacement cases would be necessary to describe the behavior.

2.4.4. Analytical Solution Conclusion

Based on the stress and displacement equations above in section 2.4.1 through 2.4.3, we have 10 analytical models, each with an increasing number of eigenvalues and constants implemented (two models for each complex λ value and one model for each real λ value). As the parameters in the model increase, the stress field in which the model is valid also increases. These models are collocated with boundary element data to estimate the parameters. Then, the estimation of the first two parameters will be used in a singular model to determine to singularity dominated zone.

CHAPTER 3

NUMERICAL ANALYSIS FOR STRESSES, DISPLACEMENTS, AND THE SINGULARITY DOMINATED ZONE

3.1. Introduction To Determining The Stress Intensity Factor

Several techniques for determining the stress intensity factor have been implemented over the years. If a solution to the stress intensity problem cannot be found in a handbook or accurately approximated, then one of three techniques are typically implemented: exact solutions, experimental solutions, numerical solutions. Each method is discussed briefly.

There are several noteworthy exact solution methods. For example, the alternating method has been used to extract a solution when there are two or more similar problems which have an exact solution known. In this case, the known solutions have the same geometry of stress raisers, but different loading conditions. They are super-positioned in a strategic way to provide a solution to a different problem. This has been useful for three-dimensional problems as well (19).

In 1974, Cartwright and Rooke proposed a similar method called the compounding method (20). This method involves the summation of different known stress raiser problems. In essence, the loading is fixed, but the geometry different for each summed solution. Other, more complex, proposed solutions are the transformation methods of Sneddon and Lowengrub (21) and the Laurent series expansions (22). However, for most problems, an exact solution is not possible; therefore numerical methods and experimental methods are widely used.

Experimental methods are extensively used in research to find the stress intensity factor. The main approaches are photoelasticity, moiré, caustics, and strain gage methods. Except for the strain gage method, all the previously mentioned techniques use optics. Photoelasticity is the most widely used full-field method, and essentially began when Irwin (23) observed that isochromatic fringes near a crack tip formed closed loops and were tilted away from the vertical (due to the σ_{ox} , or T-stress (24)). These fringes are contours of maximum in plane shearing stress. When used in conjunction with a collocation scheme, the stress intensity factor may be determined, as shown by Sanford and Chona (25), and Etheridge and Dally (26). For a review of early photoelasticity research, the reader is referred to Dally (27).

The method of caustics uses the deflection of light rays from high stress-field gradient near the crack tip and was first proposed by Mannog in 1964 (28). Since then, many others have contributed to this approach, such as Philips and Sanford, and Kalthoff (29, 30). The moiré method uses fringes to measure the displacements, to which Barker, Sanford, and Chona have obtained experimental results (31). Finally, strain gages work by changing resistance when a strain is applied to it. While this method is widely used in many applications, it drew early criticisms in fracture mechanics due to the high stress gradients near a crack tip. However, this can easily be overcome by moving the strain gages outside of the SDZ and using a few higher order terms to describe the behavior. Furthermore, by using a pair of symmetrically placed gages, mixed mode stress intensities can be found (32, 33).

The three main numerical approaches to determining stress intensity factors are the boundary collocation method, the finite element method, and the boundary element method. Boundary collocation involves the application of remote boundary conditions being discretely satisfied. This gives known stresses along the boundary that a fitting

function can be performed on. To reduce error, Hulbert showed that a large number of data points must be taken along the boundary (34). Further discussion into the collocation schemes will be given in section 3.3.

The finite element method splits the problem into many small parts, defined by nodes. It then assumes a shape and stress distribution between the nodes. Around the crack tip, many nodes must be taken at the expense of computational time (36). Much work has gone into optimizing this technique (37, 38, 39, 12). Finally, the boundary element method has gained recent interest in fracture mechanics. It is described in detail in section 3.2.

3.2 Boundary Element Method

Boundary element solutions reduce a two-dimensional problem to a one dimensional problem. The boundary element formulation is based on Green's function for an anisotropic bimaterial is used (40). The boundary element solution is superior to finite element near the interface due to the inherent singularity near the interface. Furthermore, in the boundary element used in this thesis (18), the interface continuity conditions are satisfied analytically and do not need to be discretized. The displacement boundary integral equation is

$$u_j(p) = \int_{\Gamma} U_{ji}(p, Q)t_i(Q)d\Gamma - \int_{\Gamma} T_{ji}(p, Q)u_i(Q)d\Gamma \quad (3.1)$$

where p is the source point. $U(p, Q)$ and $T(p, Q)$ are the two point displacement and traction Green's functions, respectively, and Q is the field point on the boundary. $t(Q)$ and $u(Q)$ are the tractions and displacements, respectively, at the boundary point Q .

Similar to Martin's formulation, the stresses are derived from the displacements (whereas the our analytical stresses, chapter 3, are formed from the Airy Stress function and the displacements were derived from the constitutive relationship and the stresses). The formulation of the stresses for the boundary element solution is

$$\sigma_{ij}(p) = \int_{\Gamma} D_{jik}(p, Q) t_k(Q) d\Gamma - \int_{\Gamma} S_{jik}(p, Q) u_k(Q) d\Gamma \quad (3.2)$$

where indices i and j are the faces and direction, respectively, of a differential stress element of the source point p . $D(p, Q)$ and $S(p, Q)$ are the two point displacement and traction Green's functions, respectively, of p and Q . They are third rank tensors from the derivatives of the traction and displacement kernels from equation 3.2. $t(Q)$ and $u(Q)$ and Q are described above. Further details can be seen in Kane (41).

The integrals are discretized along the boundary. Therefore, similar to the finite element method, there exists an optimization problem of balancing computational time versus resolution. For our boundary element method analysis, a specimen of dimensions 100 by 200 (in arbitrary units) for each material is chosen as shown in Figure 3.1. The interface is along the x direction at y equals zero. The internal points are shown to be taken at the interface free edge. Also, no boundary element data points exist along the interface.

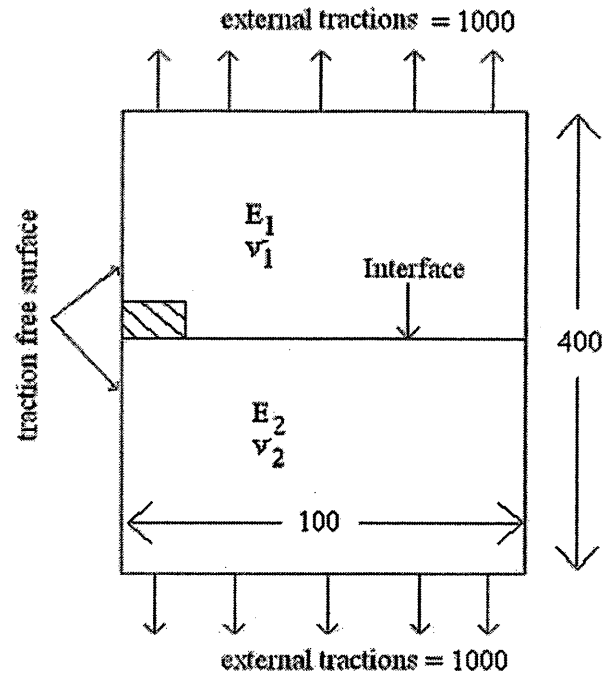


Figure 3.1: Schematic Of Boundary Element Model.

As part of the boundary element solution, stress and displacement are computed at internal points shown as the rectangle of points near the interface corner in Figure 3.1. The internal boundary element method stresses and displacements are fitted to the analytical stresses and displacements shown in section 3.4 and the stress intensity estimated.

3.3 Local Collocation

In order to solve for the unknown parameters in the analytical model described in section 3.4, a fit to data must be performed. The local collocation scheme is widely accepted as an accurate technique of determining the stress intensity (42). In addition, a convergence plot of the leading term verses the number of parameters in the model is used as the

criterion for the solution, similar to Sanford's example of a boundary collocation problem of a single-edge notched geometry loaded in uniform tension (1). His converged value matched those of Tada, Paris, and Irwin's empirical result (43). Furthermore, a root mean square relative error equation is used to validate the model's fit as

$$error = \frac{100}{N} \sqrt{\sum_{i=1}^N \left(\frac{\sigma_i^d - \sigma_i^m}{\sigma_i^d} \right)^2} \quad (3.3)$$

where σ_i^d is the boundary element data, σ_i^m is the model, and N is the number of data points.

The general form of our local collocation scheme is an overdetermined set of linear equations,

$$A\bar{x} = \bar{b} \quad (3.4)$$

where \bar{x} and \bar{b} are vectors, while A is a matrix. For the problem, \bar{b} is the column of known internal displacements obtained from the boundary element points, which takes the form

$$\bar{b} = \begin{pmatrix} u_j(r_1, \theta_1) \\ u_j(r_2, \theta_2) \\ u_j(r_3, \theta_3) \\ \vdots \\ u_j(r_{N-1}, \theta_{N-1}) \\ u_j(r_N, \theta_N) \end{pmatrix} \quad (3.5)$$

where r_i and θ_i are the locations of the data. For this analysis, the displacement data is taken very close to the interface free-edge intersection.

In equation (3.4), \bar{x} is a column vector of the unknown coefficients in the series expansions of the stresses,

$$\bar{x} = \begin{pmatrix} C_1 \\ C_2 \\ C_3 \\ \vdots \\ C_{M-1} \\ C_M \end{pmatrix} \quad (3.6)$$

where C are unknown parameters and M is the total number of unknown parameters in the model. Finally, the A matrix is filled with the results of the analytical models from section 2.4 at specific points, excluding the unknown coefficients. The analytical stress models take the form $\sigma_{mn} = C_m h_m(r_n, \theta_n)$; therefore, the matrix is

$$A = \begin{bmatrix} h_1(r_1, \theta_1) & h_2(r_1, \theta_1) & h_3(r_1, \theta_1) & K & h_{M-1}(r_1, \theta_1) & h_M(r_1, \theta_1) \\ h_1(r_2, \theta_2) & h_2(r_2, \theta_2) & h_3(r_2, \theta_2) & K & h_{M-1}(r_2, \theta_2) & h_M(r_2, \theta_2) \\ h_1(r_3, \theta_3) & h_2(r_3, \theta_3) & h_3(r_3, \theta_3) & K & h_{M-1}(r_3, \theta_3) & h_M(r_3, \theta_3) \\ \vdots & \vdots & \vdots & \vdots & \vdots & \vdots \\ h_1(r_{N-1}, \theta_{N-1}) & h_2(r_{N-1}, \theta_{N-1}) & h_3(r_{N-1}, \theta_{N-1}) & K & h_{M-1}(r_{N-1}, \theta_{N-1}) & h_M(r_{N-1}, \theta_{N-1}) \\ h_1(r_N, \theta_N) & h_2(r_N, \theta_N) & h_3(r_N, \theta_N) & K & h_{M-1}(r_N, \theta_N) & h_M(r_N, \theta_N) \end{bmatrix} \quad (3.7)$$

Because the system of equations is overdetermined, a simple inverse solution is not possible for this type of problem; therefore, several routines have been used to solve this

set of equations. One approach to solving the linear least squares problem is by using the normal equations (44). The normal equations yield a least squares solution to equation (3.4) as

$$\bar{x} = (A^T A)^{-1} A^T \bar{b} \quad (3.9)$$

However, the normal equations lead to a very ill conditioned system and large errors will occur in solving (3.9) if the order of the model is large. In this case, several other approaches can be used.

Some other methods for solving linear least squares problems are the pseudoinverse (44), QR Decomposition (35, 45), and Linear Regress Fit (44, 46). All methods were used in the thesis and yielded identical results.

The Pseudoinverse works by minimizing the sum of the squares (3.10) in the expression $[A].[A]^T - I$, where I is the identity matrix. The QR Decomposition was investigated by Sanford and Berger (35), who found it to be more beneficial for certain problems in boundary collocation. It is based on an orthogonalization process of writing A as a product of $Q^T R$, where Q is an orthonormal matrix and R is a triangular matrix.

For linear parameter relationships such as ours ($Af(r, \lambda, \theta) + Bf(r, \lambda, \theta) + Cf(r, \lambda, \theta) + \dots$), a linear fit can be performed. The Linear Regress least square fit routine in this thesis is a Mathematica formulated fitting function. It is based off a simple linear least squares fit with additional features, such as automatic output of the variance table, mean squared variance, and options of adjusting the confidence level and tolerance. Linear least squares works by having the program estimate the unknown coefficients by minimizing the residual sum of squares defined as

$$R^2 = \sum_{i=1}^N (\sigma_i^d - \sigma_i^m)^2 \quad (3.10)$$

where σ_i^d is the boundary element data, σ_i^m is the model, and N is the number of data points.

While, local collocation is most often used to determine a stress intensity factor, the h-integral is a recent approach that has gained support. Based on a Green's function, it works with finite element and boundary element data requiring fewer computations than typical local collocation schemes. Labossiere and Dunn have shown its validity for certain configurations (13, 47). The h-integral is defined as

$$H = \int (\sigma_{ij} u_i^* - \sigma_{ij}^* u_i) n_j ds = 0 \quad (3.11)$$

where σ_{ij} and u_i are the actual stresses and displacements. In our case, these are analogous to the boundary element data. Also, u_i^* and σ_{ij}^* are defined as the complementary fields that satisfy the boundary conditions, equilibrium equations, and constitutive relationships. In our case, these are analogous to the analytical solutions. Furthermore, n_j is the outward unit normal to the counter-clockwise contour Γ . When the contour encloses a region just outside the singularity, H is equal to zero. As the enclosed region is shifted toward the discontinuity, the value of H can be scaled to equal the stress intensity.

For our problem, the only means of evaluating the h-integral results would be to compare it to the boundary element data for accuracy. To confidently show the stress intensity for our problem, given our small singularity, an extremely fine mesh would have to be

implemented, beyond the feasibility of this study. In contrast, the local collocation approach can accurately determine the stress intensity from the convergence criterion. Furthermore, another disadvantage of the h-integral is that to determine the singularity dominated zone, a divergence from the actual boundary element data must be used, again requiring a very fine mesh to describe our singularity. The superiority of the local collocation, using higher order terms to determine the SDZ is discussed in chapter 4.

3.4 Singularity Dominated Zone

The singularity dominated zone is a very small region around a crack tip or other stress singularity where the stresses are adequately described by a single parameter, the stress intensity factor. As one moves outside the SDZ, higher-order terms in the series expansions are needed to accurately describe the region, as shown in Figure 3.2.

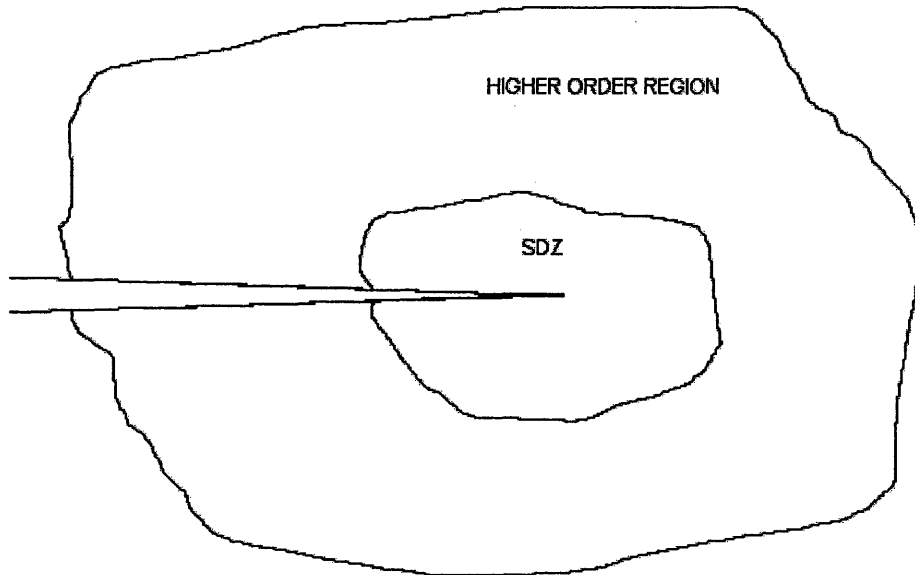


Figure 3.2: The Singularity Dominated Zone (SDZ) Surrounding A Crack Tip.

This concept was first introduced by Irwin (48). In this region, the stress gradients are often very large and singular in nature, with the strength of singularity determined by the stress intensity factor. Furthermore, the SDZ is dependent on the relative crack size, as shown by Chona, Irwin, and Sanford (49) for modified compact tension and cantilever beam specimens. The critical stress state criteria of failure, as previously stated, says that if the stress inside the SDZ is greater than the material's critical value of resistance, a crack will propagate. Therefore, the SDZ is an important aspect of fracture mechanics.

To compute the SDZ for our bimaterial problem, we will use a 20-parameter model as our full field solution, then estimate the SDZ based on a 2% difference between the singular stress and the full-field stress. Knowing that the SDZ is very small, only data near the interface free-edge is collocated. Figure 3.3 shows an example of data taken in a small region of the sample shown in Figure 3.1, where the origin is the interface free-edge corner. A solution based off this small set of data is assumed to be the full field solution, whereas the SDZ will be a minute portion of this field.

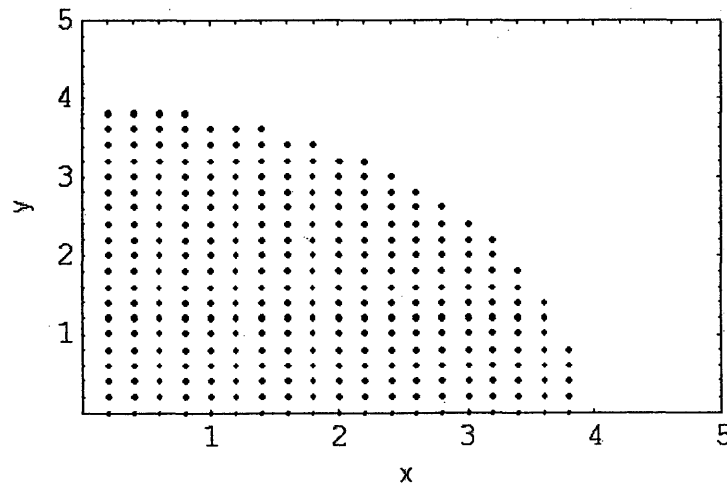


Figure 3.3: Internal Data Points In A Small Region.

CHAPTER 4

RESULTS AND DISCUSSION

4.1 Collocation

A collocation method was used to determine the coefficients in the series expansions for stresses as discussed in the previous chapter.

Knowing the singularity dominated zone is a very small region near the interface free-edge corner in boundary element data, a small radius in the upper material was collocated. Research from other papers was used to aid in an initial estimate of what values to use. Akisanya and Meng investigated the interface free-edge of two materials bonded by an adhesive. They found that the singular elastic field, based on a 2 percent difference between the asymptotic solution and the finite element solution, to be a radius of between 0.02 and 0.15 times the adhesive layer thickness (15). Ding, Meekisho, and Kumosa analyzed a similar problem with the finite element iterative method and determined the singularity dominated zone for various configurations. Using a stress-based criterion, the SDZ was shown to be between .04 and .17 times the adhesive layer thickness (12, 50). Furthermore, Chona, Irwin, and Sanford (49) found the minimum SDZ for a common fracture test specimen to be approximately .01 times the specimen's width minus crack length.

The boundary element data for our problem was obtained by assuming dimensions for the upper and lower material of a height equal to 200 and a width of 100. Figure 3.1 shows the schematic of the specimen. External tractions of 1000 are applied on the upper and lower boundary at these points in accordance with the problem shown in Figure 2.1.

Also, the left interface free-edge has a fixed displacement. The units are arbitrary, since all calculations were normalized. Stress data was obtained in a region of radius 4.5 (approximately .02 times the height of the upper material) to use in the collocation analysis.

For collocation of our analytical model to our boundary element data, the radius in the analytical model was normalized. Chona, Irwin, and Sanford used this normalization in their study of the SDZ with respect to specimen size and shape (50). Labossiere and Dunn also used a normalized variable w in their calculations of mixed-mode stress intensities in a glass-silicon interface (13, 47). For convenience, the parameter w is often defined as the width of the specimen, but this is not required. For our problem, w was selected to be 10^5 .

The local collocation scheme leads to an overdetermined system, where the number of data points must be greater than the number of unknown parameters. For boundary collocation, a redundancy of between 2 and 5 is sufficient to obtain quality results (1). For local collocation, Chona, Irwin, and Sanford used a redundancy of 20 for their calculations (50). Thus, a redundancy of 19 was selected for our problem.

4.1.1 Convergence Results

The convergence plot for the first two terms in the stress expansions is shown in Figure 4.1. The convergence is clearly shown and both coefficients are related in magnitude by a ratio of 1 to 1.5. The convergences of the 3rd and 4th terms are also plotted in Figure 4.2. The magnitudes of the all the first four terms are close to each other relative to the remaining values. Figure 4.3 shows the convergence of the first four terms plotted together.

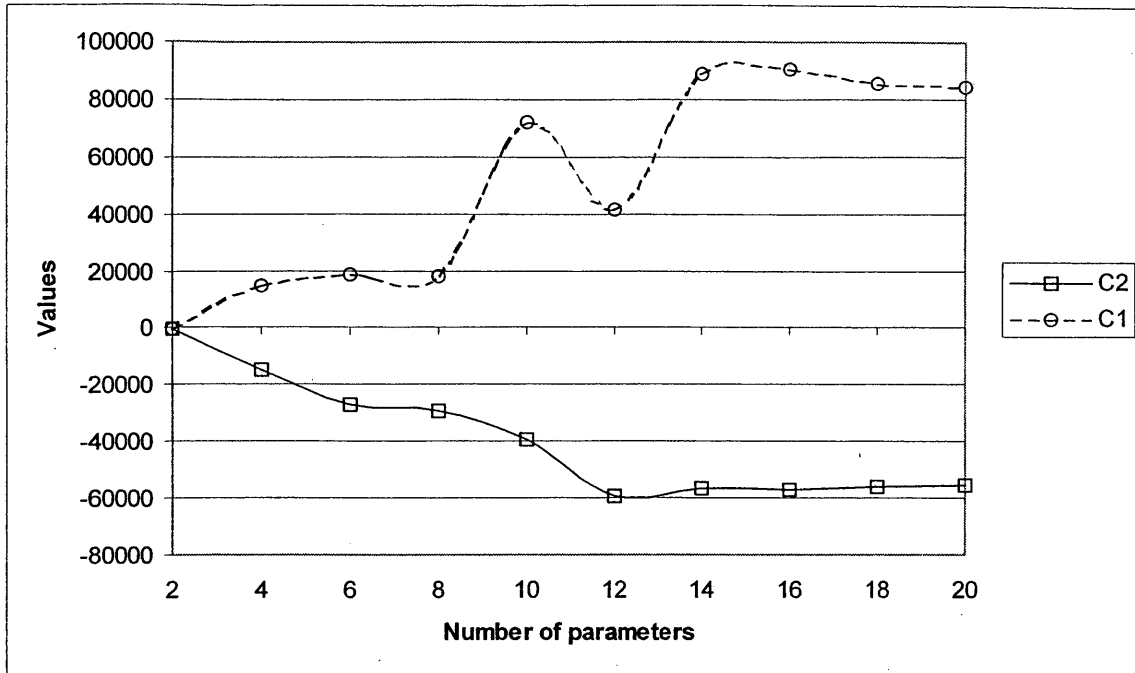


Figure 4.1: Convergence Of The First Two Leading Terms, C1 And C2.

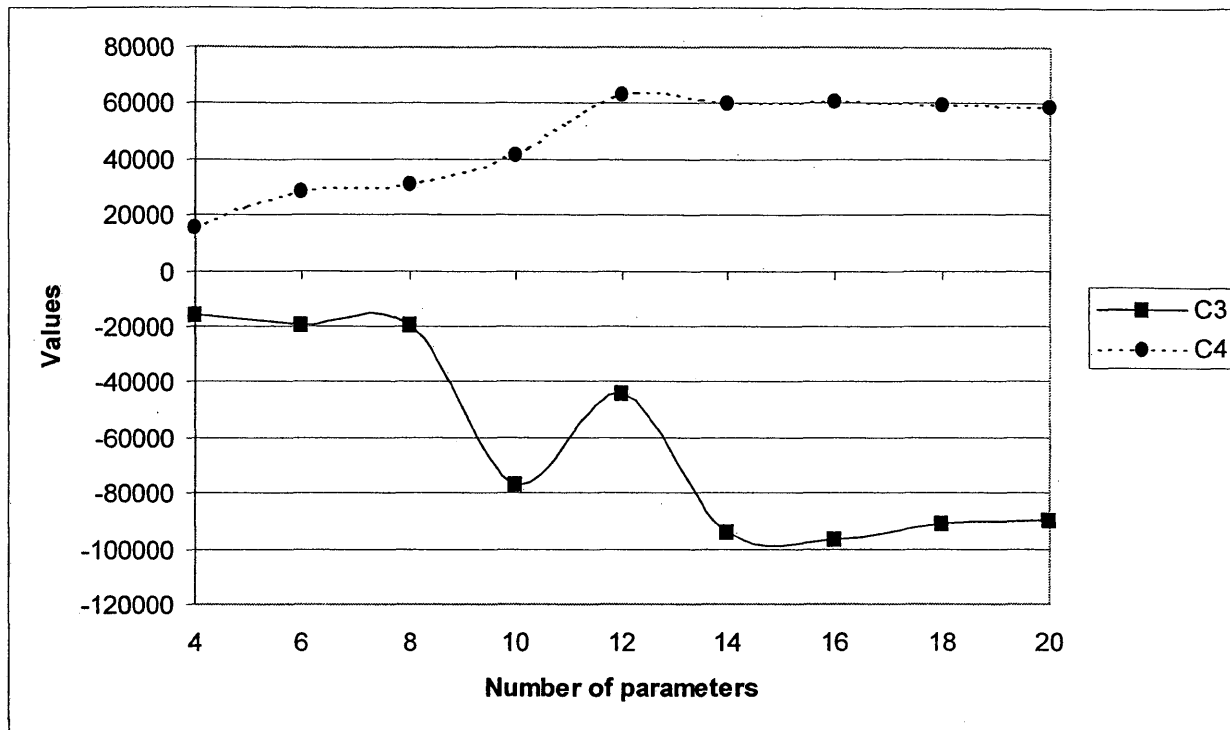


Figure 4.2: Convergence Of The Third And Fourth Terms, C3 And C4.

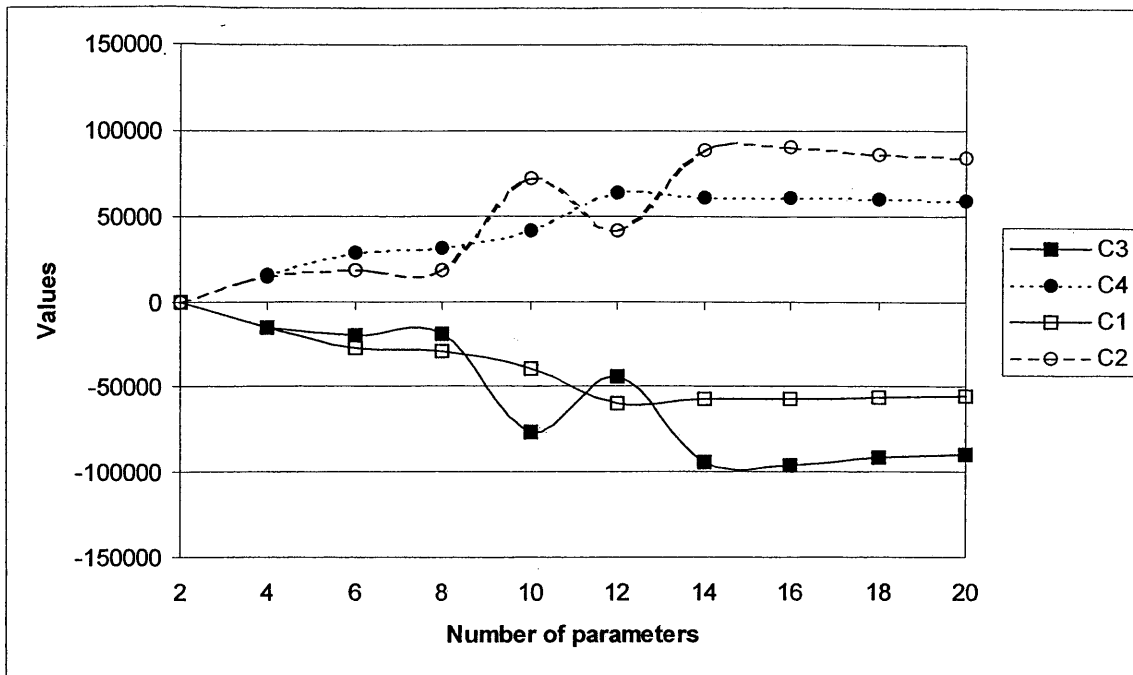


Figure 4.3: Convergence Plot For C1 Through C4.

The previous Figures show that convergence is reached for the first four terms with a 14-parameter model. The terms for C5 and higher may not have convergence. Table 4.1 shows these results. The dimensions are in terms of stress times the square root of a length (typically, $\text{psi (in)}^{1/2}$ or $\text{MPa (m)}^{1/2}$).

Table 4.1: Local Collocation Values Of The Normalized Coefficients.

Terms 1-10	Value	Terms 10-20	Value
C1	-55341.2	C11	2.1×10^{12}
C2	84451.8	C12	-1.1×10^{12}
C3	-89697.1	C13	8.4×10^{12}
C4	58982.4	C14	8.8×10^6
C5	3.4×10^8	C15	4.8×10^8
C6	9.6×10^7	C16	-6.3×10^8
C7	-3.1×10^7	C17	-18074.8
C8	7.3×10^7	C18	-18453.8
C9	2.9×10^{12}	C19	-8461.0
C10	2.1×10^{12}	C20	8346.9

4.1.2. Accuracy Of Results

A relative error plot was made to determine the accuracy of the various order models to the boundary element data. The relative error is defined by equation (3.3). Figure 4.4 illustrates that the more parameters used in the stress model, the greater the accuracy of the model. Our 20-parameter model falls within 4 percent of the boundary element data that was collocated. At 6-parameters, a quick drop in error exists. Looking at Figure 4.3, it shows that convergence is not reached until between 12 and 14 terms are used in a model. Therefore, any oscillations that occur in the relative error for models smaller than 14-terms are due to the fitting routine used. In our case, it is interesting to note that the drop in relative error for the 6-parameter model corresponds to the first inclusion of a complex eigenvalue. There is a definite correlation between the relative error settling at the 12-parameter model, and the convergence in Figure 4.3 reached between the 12 and

14 parameter. This relationship, and the oscillations in the error function, matches those shown by Sanford for a single-edge notched boundary collocation problem (1).

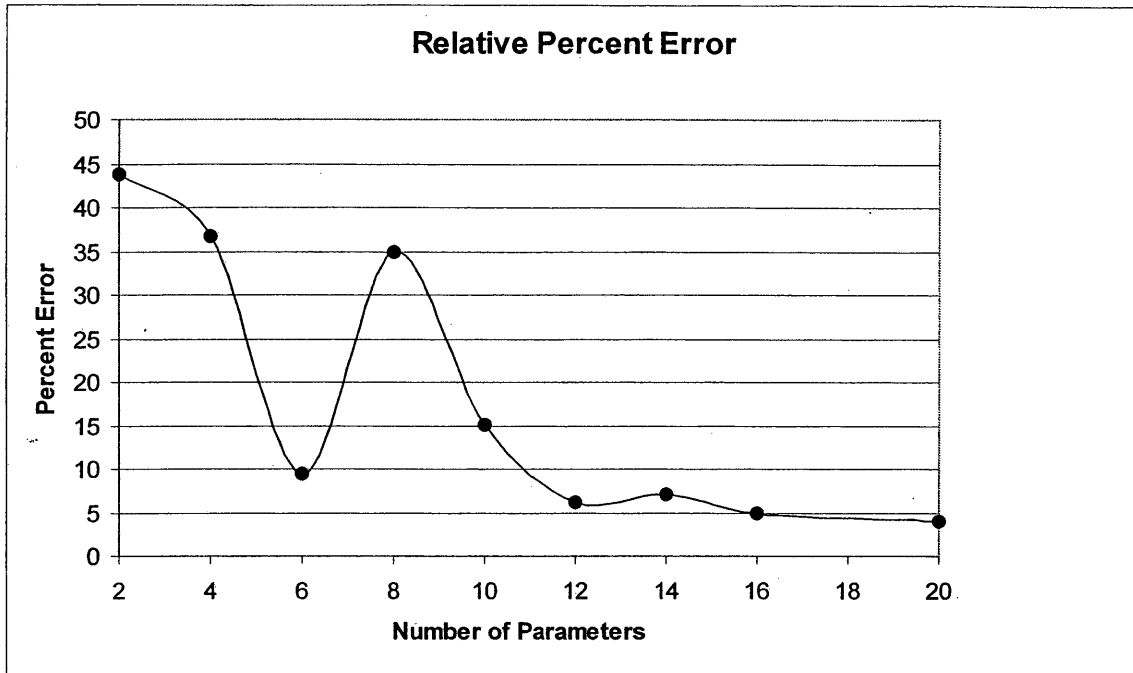


Figure 4.4: Relative Error Vs. Number Of Parameters.

In Figures 4.5a through 4.5d, the different order models are shown plotted against the actual boundary element data points along the interface. The plots are sequential snapshots zooming toward the corner of the specimen. The horizontal axis is the normalized radius. The vertical axis is the radial stress. The dark line is the model utilizing 2 terms. The light line is the 20-parameter model. The points are the boundary element data points. In Figures 4.5c and 4.5d, the singular model is shown with a dark horizontal line. The plot range is listed below the Figure number. The plots graphically show the superiority of the higher parameter model to the singular model far away from the corner. Furthermore, the singular natures of the models are clearly visible close to the

corner. The singularity of the singular model is at a very small radius; and therefore, it appears horizontal in the comparison plots. Figure 4.6 is a snapshot that shows the full behavior of the singular model.

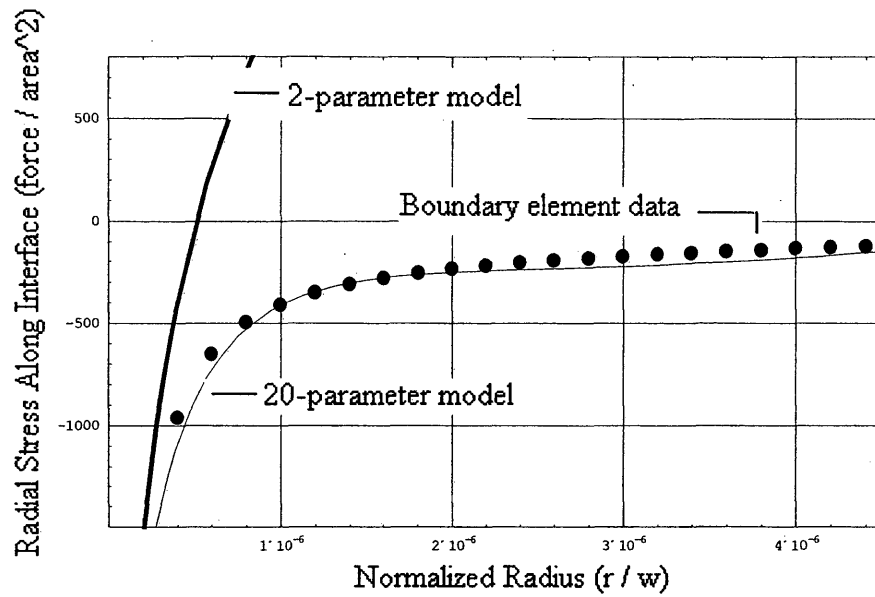


Figure 4.5a: Model Comparisons For σ_{rr} , $0 \leq r/w \leq 4 \times 10^{-4}$.

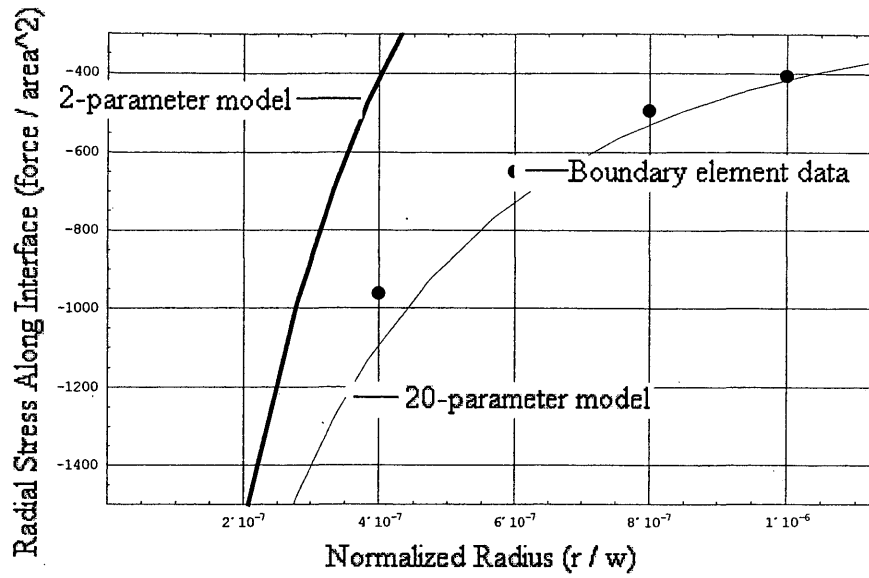


Figure 4.5b: Model Comparisons For σ_{rr} , $0 \leq r/w \leq 1 \times 10^{-6}$.

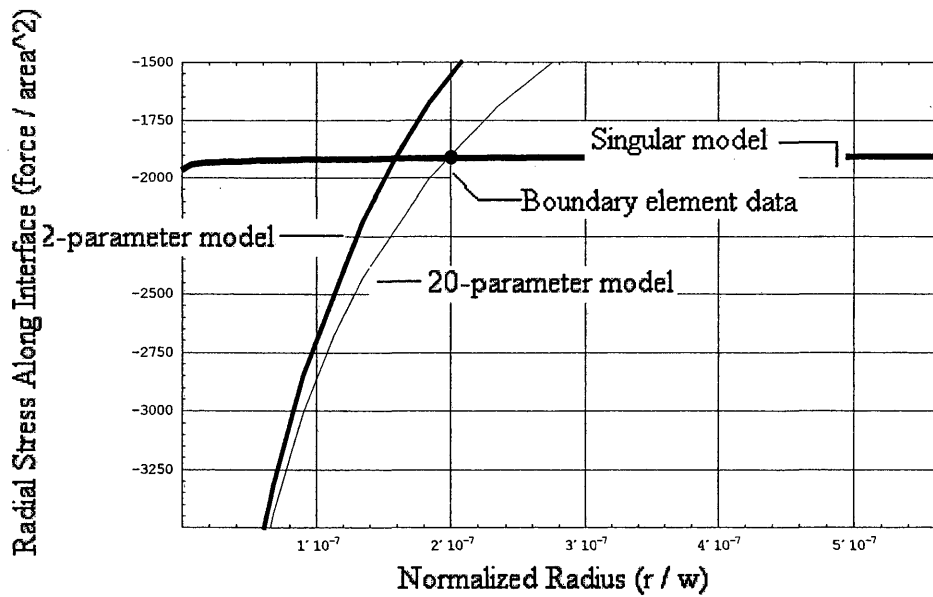


Figure 4.5c Model Comparisons For σ_{rr} , $0 \leq r/w \leq 5 \times 10^{-7}$.

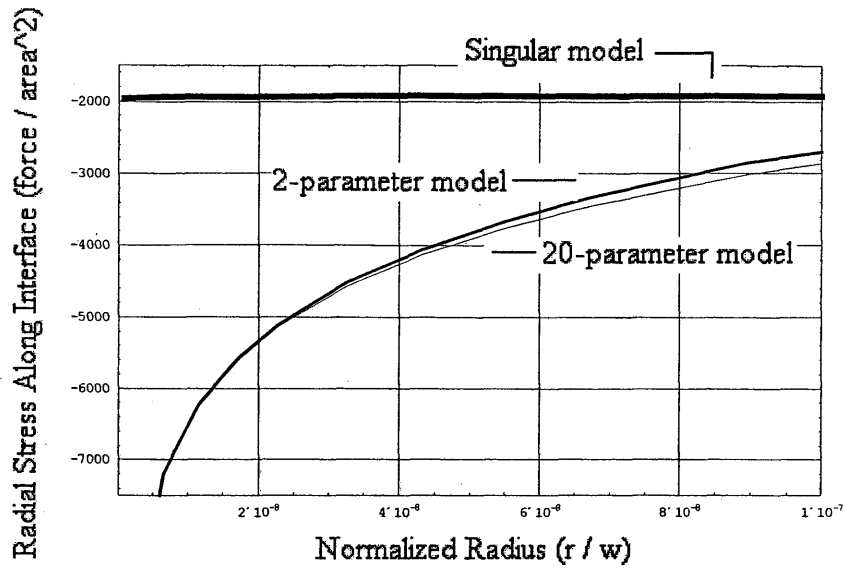


Figure 4.5d: Model Comparisons For σ_{rr} , $0 \leq r/w \leq 1 \times 10^{-7}$.

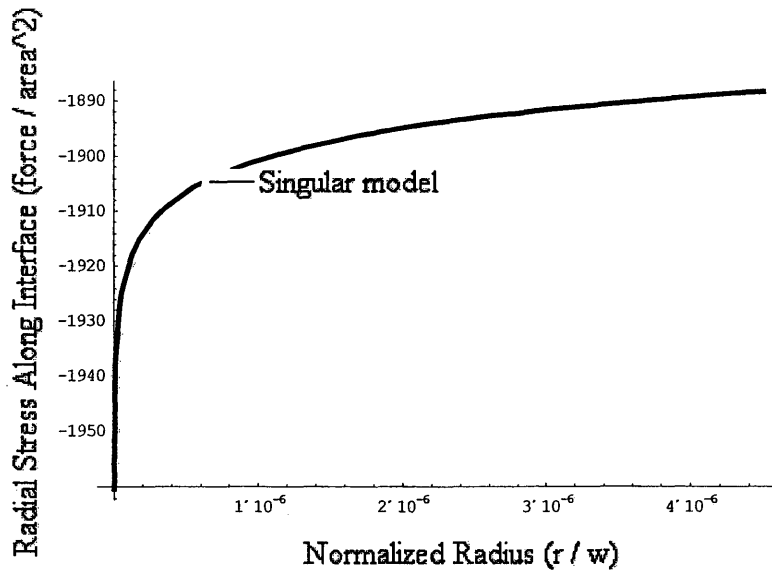


Figure 4.6: Singular Model Behavior For σ_{rr} , $0 \leq r/w \leq 4 \times 10^{-6}$.

4.1.3. Stress Intensity Factor

In determining the stress intensity factor of this problem, several principles were considered. The convergence values found were based on a normalized radius.

Therefore, the actual converged constants, C_1^1 and C_2^2 , are defined as

$$C_1^1 = w^{\lambda_1-1} C_1 \quad (4.1)$$

$$C_2^2 = w^{\lambda_1-1} C_2 \quad (4.2)$$

where w is the normalization factor (10^5 for our problem) and λ_1 is the first singular eigenvalue (.995 for our problem). Based on this, C_1^1 equals $-51,647$ and C_2^2 equals $78,815$. Similarly, C_3^3 equals $-89,697$ and C_4^4 equals $58,982$. Again, these dimensions are stress times the square root of a length. Now that the converged constants are determined, the stress intensity factor can be found.

In general, the stress intensity factor is a function of the applied stress and geometry. For example, in an infinite plate under tension with a central crack, the stress intensity factor is defined as $K = \sigma\sqrt{\pi a}$, where σ is the applied stress and a is half the crack length.

For a bimaterial, however, the stress intensity is ultimately a function of applied stress, geometry, and Dundurs parameters. The Dundurs parameters are variables in the determination of the stress intensity because the ratio of material properties affects the behavior of the specimen. The eigenvalues reflect the dependence on the material properties, as shown in chapter 2. For a detailed study on this, the reader is directed to Ding and Kumosa (12), who also defined the general stress and displacement state as

$$\sigma_{ij} = K r^{\lambda_1 - 1} f_{ij}(\theta) \quad (4.3)$$

$$u_i = K r^{\lambda_1} g_i(\theta) \quad (4.4)$$

where K is the stress intensity, λ_1 is the singular eigenvalue, and f and g are the trigonometric components of the stress, eqs. (2.8)-(2.10), and displacement, eqs. (2.20) and (2.21), respectively. For our problem, the stress intensity is related to the first two converged constants by the relationship

$$K = \sqrt{C_1^2 + C_2^2} \quad (4.5)$$

where C_1^1 and C_2^2 are the converged coefficients. K is equal to 94,230, with the same dimensions as the constants listed in Table 5.1. In the normalized form,

$$K = 101 \sigma_0 w^{\lambda_1 - 1} \quad (4.6)$$

where σ_0 is remote stress and w is the normalizing parameter, and λ_1 is the first singular eigenvalue. For the crack problem, C_1^1 and C_2^2 separate into functions of sine and cosine respectively, as follows

$$\begin{aligned} \sigma_r = & \frac{C_1^1}{4\sqrt{r}} \left(5 \cos \frac{\theta}{2} - \cos \frac{3\theta}{2} \right) + \frac{1}{2} \sigma_{ox} (1 + \cos(2\theta)) + \\ & \frac{C_2^2}{4\sqrt{r}} \left(-5 \sin \frac{\theta}{2} + 3 \sin \frac{3\theta}{2} \right) + H.O.T \end{aligned} \quad (4.7)$$

where r is the radius, $\sigma_{0,x}$ is the T-stress and $H.O.T.$ are the higher order terms. The cosine portion relates to the opening mode fracture and the sine portion relates to the forward shear mode fracture (6, 1). Our problem, however, does not break up into the fracture modes as neatly as equation (4.7). Therefore, the approach of Ding and Kumosa must be taken (12). This relationship, described by equations (4.3) and (4.5), simplifies the stress equations (2.8)-(2.10) into the stress intensity and corresponding geometric function. Because of the form of equations (2.8)-(2.10), mixed mode fracture is assumed. For further investigation on mixed mode fracture in bimetals, the reader is referred to Labossiere, P., Dunn, M., and Cunningham (13). Since the focus of this thesis is on the singularity dominated zone, a mixed mode fracture study is omitted, only the stress intensity is defined.

4.2. Singularity Dominated Zone

The SDZ is the small region where the stresses, strains, and displacements are dominated by the singular term in stress. In a perfectly bonded material without defects, fracture will initiate at the free-edge interface in this region. Disregarding plasticity, the stresses and displacements are completely described by equations 4.3 and 4.4 above. Therefore, it is imperative to know the size of the region of validity of these equations. The boundary of the SDZ is taken to be when the radial component of equation 4.3 deviates from the 20-parameter radial stress model by 2 percent.

In studying a homogenous crack problem, Chona, Irwin, and Sanford showed the small singularity dominated zone of a one-parameter model and noted the importance of including the constant-stress terms in the crack-tip stress field. Also, they showed that as the crack grows and approaches the boundary, the constant stress relaxes and the SDZ

increases in size (49). Furthermore, the influence of the constant-stress term affects plasticity, as shown by Larsson and Carlsson (51). For further studies into the constant-stress behavior, the reader is directed to references (52, 53, 54).

Because of the strong influence of the constant stress case, the 2-term expansion, which includes the singular model and the constant stress model, was determined to be most important and practical for study. Because of precision limitations; the size of the singularity dominated zone is too small for Mathematica software to determine it. For example, along the interface, where the constant stress term is the most influential, the 5 percent deviation was below 10^{-400} in normalized radius. Therefore, calculations were performed using the first two roots, summing together the singular model and the constant-stress model. For the remainder of this thesis, it will be referred to as the 2-term expansion.

Figure 4.7 through 4.9 show the region of 2-percent deviation and the region of 5-percent deviation. The origin is the corner of the interface free-edge. The SDZ shown below was determined from the normalized analytical equations. Therefore, the 2 percent two-term model boundary ranged from about 2.0×10^{-8} to 4.5×10^{-8} units of length (approximately 2.0×10^{-5} to 4.5×10^{-5} times the specimen width, about 1.0×10^{-5} to 2.2×10^{-5} times the specimen height). This is three orders of magnitude smaller than SDZ studies of adhesive interfaces and cracks. The 2 percent and 5 percent shapes are linear with respect to the normalized radius, which is the same observation that Sanford found to be true in his study of the SDZ for a crack (49).

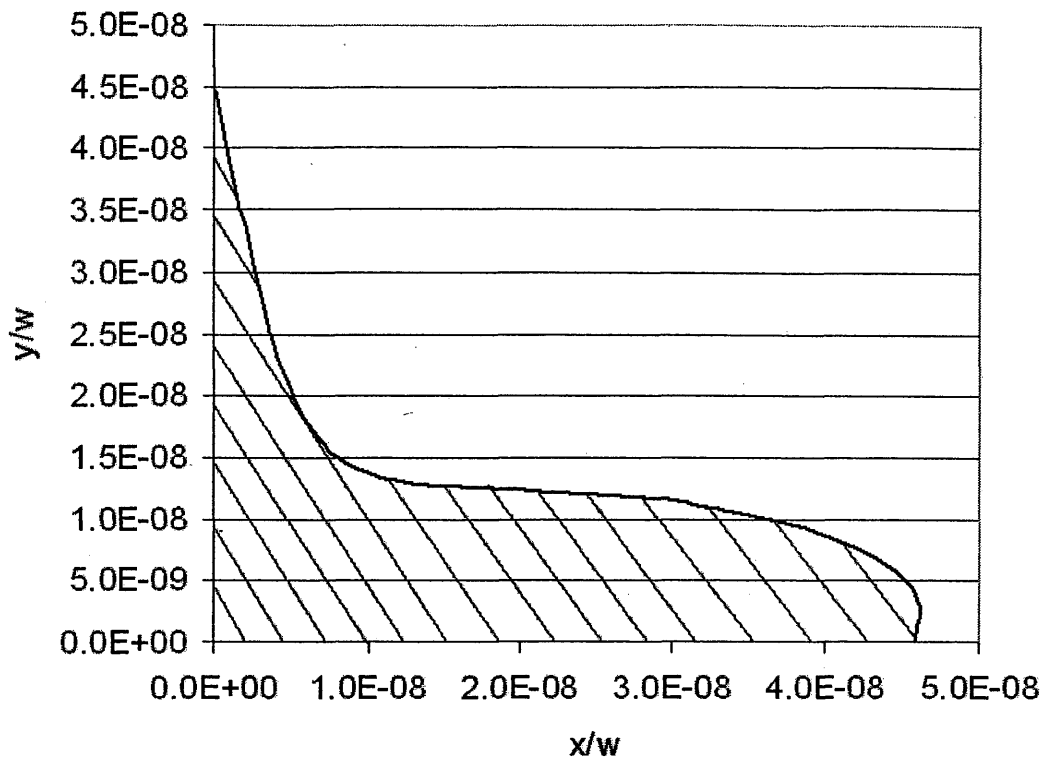


Figure: 4.7: 2% Two Term Expansion Zone.

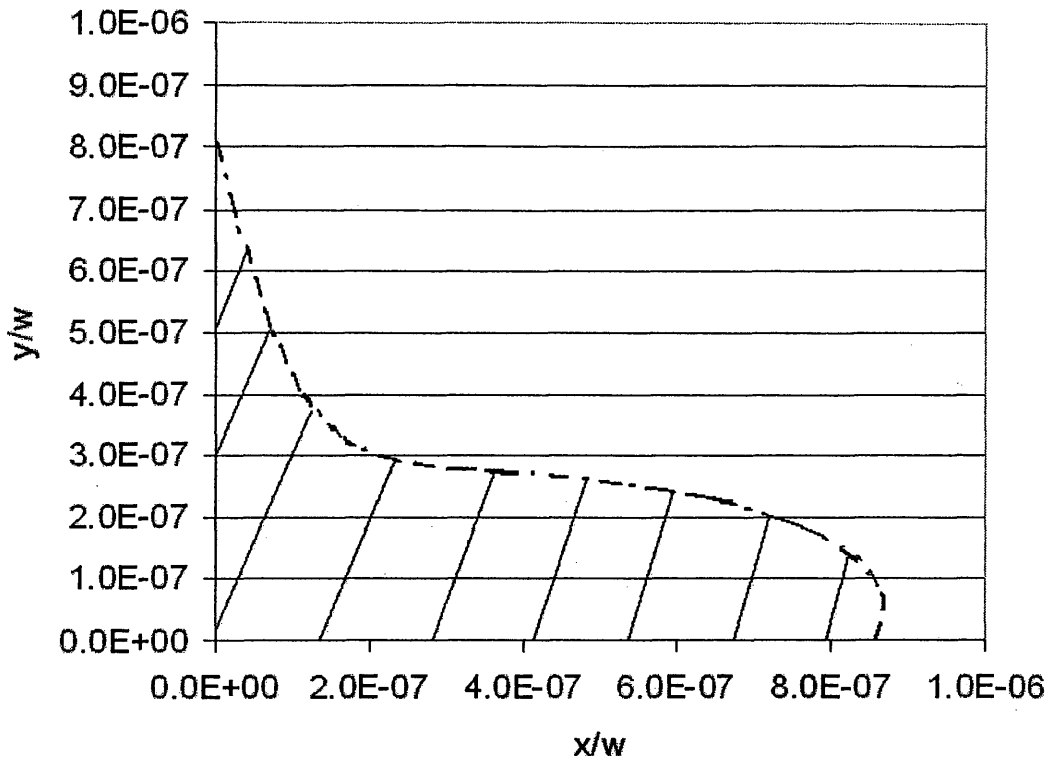


Figure: 4.8: 5% Two Term Expansion Zone.

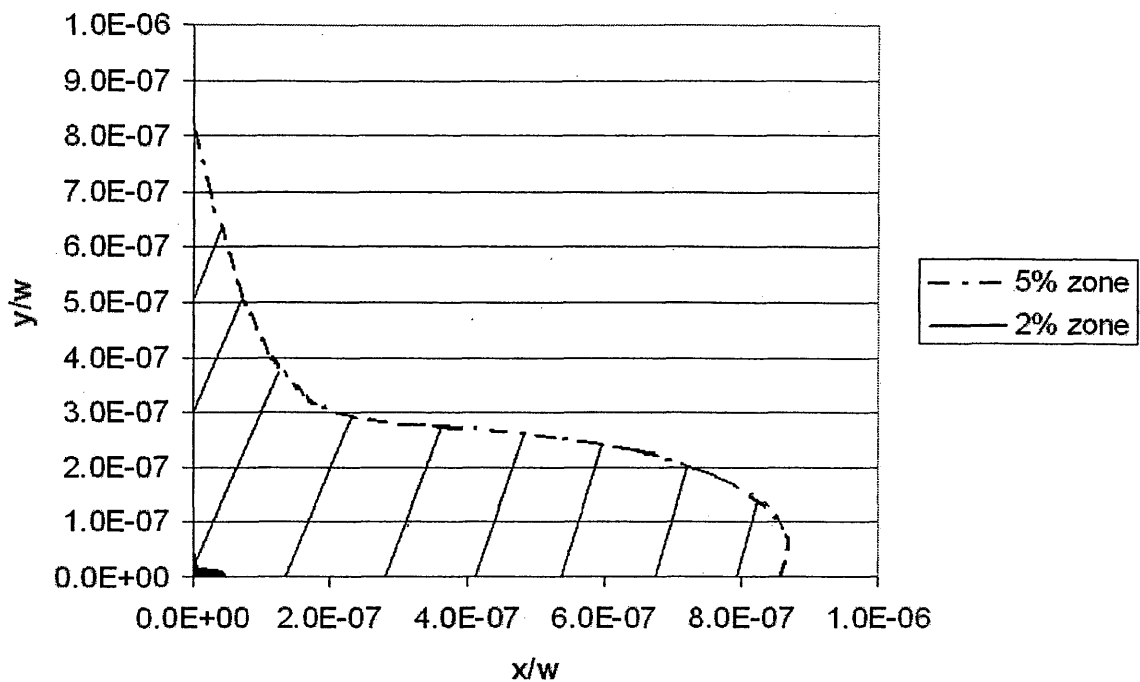


Figure: 4.9: Two Term Expansion Zone.

When units are implemented into these results, practical conclusions can be made. As an example, consider a specimen with a height of 2mm and a width of 8mm in the upper and lower materials. Under an external traction of 1000Pa, the 2-parameter zone size would be between .00033mm and .00088mm. This is found by scaling the 2-parameter zone for the dimensions in our problem to the dimensions of the example. If the applied stress were varied, the stress intensity would similarly vary. Thus, if a material toughness were known, valuable failure information could be stated. However, the 2-parameter zone would not linearly scale if the applied stress were varied, and a new calculation would have to be performed.

4.3. Discussion and Future Research

Several important comments can be made on the above results. First of all, Figures 4.5a through 4.5d reveal a scarcity of boundary element data in the two-parameter model and no boundary element data for singular portion of the singular model. This is one important difference of determining the SDZ using a divergence from higher order term model verses using a singular model divergence from raw data. Ding and Kumosa determined the SDZ with a divergence from finite element data, which required an extremely fine mesh to be implemented near the corner (12). For our problem, the 20-parameter model fit the boundary element data to 4-percent and was used as the standard. One interesting study would be to repeat our procedure using other published problems. This could provide a good comparison of finite element, boundary element, experimental data and methods determining the stress intensity and the SDZ.

Another observation that is valuable to point out is the size of the SDZ in relation to other work. In a bimaterial, as the material mismatch increases, the singularity increases. As the singularity increases, the SDZ increases also. Thus, since our interface materials are more similar in composition than that of Ding and Akisanya's adhesive bimaterial problems, it is expected that our SDZ, and 2-term expansion, be smaller. Future research could include a more complete comparison of SDZ sizes for different material combinations.

It is important to be reminded that this thesis is a determination of the stress intensity and SDZ using boundary element data only. Experimental results would be beneficial to obtain, particularly in looking at the effect of the constant-stress and plasticity. Given current manufacturing techniques, it is difficult to create such a specimen. One big obstacle is to grade the specimen without inducing defects on the free-edge. Given the

small scale of data we are interested in, another inherent difficulty is to analyze the experimental results. Currently, only Moiré methods could give an accurate result.

Finally, for future research, it would be beneficial to examine the SDZ and stress intensity based on a collocation of other stress components and displacements. Of particular interest would be the displacement equation that includes the λ equals one case. To get a complete picture of the problem, it would be helpful to analyze the bottom material of the bimaterial in addition to the upper material.

CHAPTER 5

CONCLUSION

Several important conclusions can be made from these studies. First, and most apparent, the singularity dominated zone for a copper-tungsten interface problem is very small compared to other geometry and materials that have been studied in fracture mechanics. For practical applications, the singularity is essentially non-existent mostly due to the similarity in material properties of the bimaterial. Therefore, when a crack is near the interface of a perfectly bonded copper-tungsten bimaterial with of our properties (Dundur parameters of β equal to $-.003395$ and α equal to $.070825$), the interface singularity will practically have no effect on the crack propagation.

Next, the second real root is a constant-stress term, analogous to the 'T-stress' in a crack problem. It had significant effects on the problem. Since the singularity is very close to unity, the stress intensity and the constant-stress terms are of similar values; therefore, the constant-stress must be included to accurately analyze the results in a region of practical size. The angular displacement equations from this unity root case are a function of radius in both a linear and logarithmic fashion, as $g_2(r)$ is a logarithmic function.

Finally, this study verifies the applicability of determining the singularity dominated zone and stress intensity factor without the use of extremely fine discrete data point meshes. By deriving the complex higher order stresses and eigenvalues analytically, only a limited number of boundary element data points are needed to accurately describe the behavior of the specimen.

REFERENCES CITED

1. Sanford, R. J., *Principles of Fracture Mechanics*, Pearson Education, Inc., Upper Saddle River, NJ, 07458, 2003.
2. Inglis, C.E., "Stresses in a Plate Due to the Presence of Cracks and Sharp Corners," *Transactions of the Institution of Naval Architects*, London, England, Vol. 60, 1913, pp. 219-230.
3. Griffith, A.A., "The Phenomena of Rupture and Flow in Solids," *Philosophical Transactions of the Royal Society of London*, England, Vol. 221, 1921, pp. 163-198.
4. Irwin, G.R., and Kies, J.A., "Fracturing and Fracture Dynamics," *Welding Journal*, Vol. 31, Research Supplement, 1952, pp. 95-100.
5. Williams, M.L., "Stress Singularities Resulting From Various Boundary Conditions in Angular Corners of Plates in Extension." *Journal of Applied Mechanics*, Trans. ASME, Vol.74, 1952, pp.526-528.
6. Williams, M.L., "On the Stress Distribution at the Base of a Stationary Crack", *Journal of Applied Mechanics*, Vol. 24, 1957, pp. 109-114.
7. K. Ichikawa, *Functionally Graded Materials in the 21st Century: A Workshop on Trends and Forecasts*, Boston: Kluwer Academic Publishers, 2001.

8. Bogy, D.B., "Edge-Bonded Dissimilar Orthogonal Elastic Wedges Under Normal and Shear Loading," *Journal of Applied Mechanics*, Vol.35, trans. ASME, vol.90, Series E, 1968, pp. 460-466.
9. Dundurs, J., "Discussion of Edge-Bonded Dissimilar Orthotropic Elastic Wedges under Normal and Shear Loading," *Journal of Applied Mechanics*, Vol. 36, 1969, pp. 650-652.
10. Bogy, D.B., "The Plane Solution for Anisotropic Elastic Wedges under Normal and Shear Loading," *Journal of Applied Mechanics*, Vol. 39, 1972, pp. 1103-1109.
11. Dempsey, J.P. and Sinclair, G.B., "On Singularities in the Plane Elasticity of the Composite Wedge," *Journal of Elasticity*, Vol. 9: 1979, pp.373-391.
12. Ding S. and Kumosa M., "Singular Stress Behavior at an Adhesive Interface Corner," *Engineering Fracture Mechanics*, Vol.47, No.4, 1994, pp.503-519.
13. Labossiere, P., Dunn, M., and Cunningham, S., "Application of bimaterial interface corner failure mechanics to silicon/glass anodic bonds," *Journal of the Mechanics and Physics of Solids*, Vol. 50, 2002, pp. 405-443.
14. Reedy, E.D., "Connection between interface corner and interfacial fracture analyses of an adhesively-bonded butt joint," *International Journal of Solids Structures*, Vol. 30, 2000, pp.2429 – 2442.

15. Akisanya, A.R. and Meng, C.S., "Initiation of fracture at the interface corner of bi-material joints," *Journal of the Mechanics and Physics Solids*, Vol.51, 2003, pp.27-46.
16. Sanford, R. J. and Chona, R., "Photoelastic calibration of the short-bar chevron-notched specimen," *Chevron-Notched Specimens: Testing and Analysis*, ASTM STP 855, J. H. Underwood, S. W. Frieman, and F. I. Baratta, eds., American Society for Testing and Materials, Philadelphia, Pennsylvania, 1984, pp. 81-97.
17. Martin, P.A., "On Green's function for a bimaterial elastic half-plane," *International Journal of Solids and Structures*, Vol. 40, 2003, pp. 2102-2119.
18. Berger, J.R. "Boundary Element Analysis of Anisotropic Bimaterials with Special Green's Functions," *Engineering Analysis with Boundary Elements*, Vol. 14, 1994, pp. 123-131.
19. Grandt, A.F., Harter, J.A., and Heath, B.J., "Transition of Part-Through Cracks at Holes into Through-the-Thickness Flaws," *Fracture Mechanics*, STP 833, American Society for Testing and Materials, Philadelphia, 1984, pp. 7-23.
20. Cartwright, D.J, and Rooke, D.P., "Approximate Stress Intensity Factors Compounded From Known Solutions," *Engineering Fracture Mechanics*, Vol. 6, 1974, pp. 563-571.
21. Sneddon, I.N., and Lowengrub, M., *Crack Problems in the Classical Theory of Elasticity*, John Wiley: New York, 1969.

22. Isida, M., "Method of Laurent Series Expansion for Internal Crack Problems of the Theory of Elasticity," *Methods of Analysis and Solution of Crack Problems, Mechanics of Fracture*, vol. 1, 1973, pp. 56-130.
23. Irwin, G.R., "Discussion of: The Dynamic Stress Distribution Surrounding a Running Crack – A Photoelastic Analysis," *Proceedings of the SESA*, 16(1), 1958, pp.93-96.
24. Bradley, D.B. and Kobayashi A.S., "An Investigation of Propagating Cracks by Dynamic Photoelasticity," *Experimental Mechanics*, 10(3), 1970 pp.106-113.
25. Sanford, R.J., and Chona, R., "Analysis of Photoelastic Fracture Patterns with a Sampled Least Squares Method," *Proceeding, Spring Meeting, Society for Experimental Mechanics*, May 1981, Dearborn, MI, 1981, pp. 273-276.
26. Etheridge, J.M., and Dally, J.W., "A Critical Review of Methods for Determining the Stress Intensity Factors From Isochromatic Fringes," *Experimental Mechanics*, 17(7), 1977, pp. 248-254.
27. Dally, J.W., "Dynamic Photoelastic Studies of Fracture," *Experimental Mechanics*, 19(10), 1979, pp. 349-361.
28. Mannog, P., *Anwendungen der Schattenoptik zur Untersuchung des ZerreiBvorgangs von Platten*, Ph.D. Dissertation, Ernst-Mach Institute: Germany, 1964.

29. Phillips, J.W., and Sanford, R.J., "Effect of Higher-Order Stress Terms on Mode-I Caustics in Birefringent Materials," *Fracture Mechanics: Thirteenth Conference*, ASTM STP 743, 1981, pp. 387-402.
30. Kalthoff, J.F., "Shadow Optical Method of Caustics," *Handbook on Experimental Mechanics*, 1987, pp. 430-500.
31. Barker, D. B., Sanford, R. J., and Chona, R., "Determining K and Related Stress-Field Parameters from Displacement Fields," *Experimental Mechanics*, 1985, 25(12), pp. 399-407.
32. Dally, J.W. and Sanford, R.J., "Strain-Gage Methods for Measuring the Opening-Mode Stress-Intensity Factor, K_I ," *Experimental Mechanics*, 27(4), 1987, pp. 381-388.
33. Dally, J.W. and Berger, J.R., "The Role of the Electrical Resistance Strain Gauge in Fracture Research," *Experimental Techniques in Fracture*, J.S. Epstein, Ed., Soc. Experimental Mechanics, Bethel, CT, 1993, pp. 1-37.
34. Hulbert, L.E., *The Numerical Solution of Two-Dimensional Problems of the Theory of Elasticity, Bulletin 198*, Engineering Experiment Station: Columbus, 1963.
35. Sanford, R.J., and Berger J.R., "An Improved Method of Boundary Collocation for the Analysis of Finite Body Opening Mode Fracture Problem," *Engineering Fracture Mechanics*, 37(3), 1990, pp.461-470.

36. Newman, J.C., Jr., and Raju, I.S., "Stress-Intensity Factor Equations for Cracks in Three-Dimensional Finite Bodies," *Fracture Mechanics: Fourteenth Symposium-Volume I: Theory and Analysis*, ASTM STP 791, J.C. Lewis and G. Sines, Eds., American Society for Testing and Materials, 1983, pp.238-265
37. Pu, S.L, Hussain, M.A., and Lorensen, W.E., "The Collapsed Cubic Isoparametric Element as a Singular Element for Crack Problems," *International Journal for Numerical Methods in Engineering*, Vol. 12, 1978, pp. 1727-1742.
38. Barsoum, R.S., "Triangular Quarter-Point Elements as Elastic and Perfectly-Plastic Crack Tip Elements," *International Journal for Numerical Methods in Engineering*, Vol. 11, 1977, pp. 85-98.
39. Freese, C.E., and Tracy, D.M., "The Natural Isoparametric Triangle Versus Collapsed Quadrilateral for Elastic Crack Analysis," *International Journal of Fracture*, Vol. 12, 1976, pp. 767-770.
40. Tewary, V.K., Wagoner, R.H. and Hirth, J.P., "Elastic Green's function for a composite solid with a planar interface," *Journal of Materials Research* 4, 1989, pp. 113-123.
41. Kane, James H., *Boundary Element Analysis in Continuum Mechanics*, New Jersey: Prentice-Hall, Inc, 1994.
42. Gross, B., Strawley, J.E., Brown, W.F., "Stress-Intensity Factors for a Single Edge-Notch Tension Specimen by Boundary Collocation of a Stress Function," *NASA TN D-239*, Washington, DC, Vol. 239, 1964.

43. Tada, H., Paris, P.C., and Irwin, G.R., *The Stress Analysis of Cracks Handbook*, Del Research Corporation:Hellertown, 1973.
44. <http://www.wolfram.com>, Mathematica 5, Wolfram Research, Inc, 2004.
45. Longley, J.W., *Least Squares Computations Using Orthogonalization Methods*, Marcel Dekker: New York, 1984.
46. Irwin, G.R. et al, "Photoelastic Studies of Damping, Crack Propagation, and Crack Arrest in Polymers and 4340 Steel," *NUREG/CR-1455*, University of Maryland, 1980.
47. Labossiere, P. and Dunn, M., "Stress intensities at interface corners in anisotropic bimetals," *Engineering Fracture Mechanics*, Vol. 62, 1999, pp. 555-575.
48. Irwin, G.R., "Analysis of Stress and Strains Near the End of a Crack Traversing a Plate," *Journal of Applied Mechanics*, Vol. 79, 1957, pp. 361-364.
49. Chona, R, Irwin, G.R, and Sanford, R.J., "Influence of Specimen Size and Shape on the Singularity-Dominated Zone," *Special Technical Publication, ASTM STP 791*, Vol.1, Philadelphia,1983, pp. I-3 – I-23.
50. Ding S., Meekisho, L., and Kumosa M. "Analysis of Stress Singular Fields at a Bimaterial Wedge Corner," *Engineering Fracture Mechanics*, Vol. 49, 1994, pp. 569-573.
51. Larsson, S. and Carlsson, A., "Influence of Non-Singular Stress Terms and Specimen Geometry on Small-Scale Yielding at Crack Tips in Elastic-Plastic

Materials,” *Journal of the Mechanics and Physics of Solids*, Vol. 21, 1973, pp. 263-277.

52. Eftis, J., Subramonian, N., and Liebowitz, H., “Crack Border Stress and Displacement Equations Revisited,” *Engineering Fracture Mechanics*, Vol. 9, 1997, pp. 189-210.
53. Liebowitz, H., Lee, J., and Eftis, J., “Biaxial Load Effects in Fracture Mechanics,” *Engineering Fracture Mechanics*, Vol. 10, 1978, pp. 315-335.
54. Dempsey, J.P. and Sinclair, G.B, “On the stress singularities in the plane elasticity of the composite wedge,” *Journal of Elasticity*, Vol. 9, 1979, pp.371-391.

APPENDIX

MATHEMATICA PROGRAM FOR DETERMINING EIGENVALUES IN A BIMATERIAL

1. Defining properties, material constants and angles:

```

v2 = .286;
v1 = .330;
E12 = 190 * 10^9;
E11 = 160 * 10^9;
β =  $\frac{\Gamma (k1 - 1) - (k2 - 1)}{\Gamma (k1 + 1) + (k2 + 1)}$ ;
k1 = 3 - 4 * v1;
k2 = 3 - 4 * v2;
Γ =  $\frac{E12 * (1 + v1)}{E11 * (1 + v2)}$ ;
α =  $\frac{\Gamma (k1 + 1) - (k2 + 1)}{\Gamma (k1 + 1) + (k2 + 1)}$ ;

```

2. Defining α and β with same nomenclature as Martin's paper:

```

μ2 = E12 (1 + v1);
μ1 = E11 (1 + v2);
αm =  $\frac{(1 - v1) * μ2 - (1 - v2) * μ1}{(1 - v1) * μ2 + (1 - v2) * μ1}$ ;
βm =  $\frac{(1 - 2 * v1) * μ2 - (1 - 2 * v2) * μ1}{2 * (1 - v1) * μ2 + 2 * (1 - v2) * μ1}$ ;

```

3. Determinate in Martin's paper:

```

Clear[determin];
S = -Sin[.5 * (ω * π)];
determin[ω_] = (βm^2 - 1) S^4 + (1 + 2 ω^2 (αm - βm) βm) S^2 + ω^2 (ω^2 (αm - βm)^2 - αm^2);

```

4. Do a 40-term Taylor series expansion of Sin, then define this expansion as tayS and sub into determinate equation:

```

Series[Sin[Pi / 2 ω], {ω, 0, 40}];

```

```
Clear[tayS];
```

$$\begin{aligned} \text{tayS}[\omega] = & \frac{\pi \omega}{2} - \frac{\pi^3 \omega^3}{48} + \frac{\pi^5 \omega^5}{3840} - \frac{\pi^7 \omega^7}{645120} + \frac{\pi^9 \omega^9}{185794560} - \frac{\pi^{11} \omega^{11}}{81749606400} + \\ & \frac{\pi^{13} \omega^{13}}{51011754393600} - \frac{\pi^{15} \omega^{15}}{42849873690624000} + \frac{\pi^{17} \omega^{17}}{46620662575398912000} - \\ & \frac{\pi^{19} \omega^{19}}{63777066403145711616000} + \frac{\pi^{21} \omega^{21}}{107145471557284795514880000} - \\ & \frac{\pi^{23} \omega^{23}}{216862434431944426122117120000} + \frac{\pi^{25} \omega^{25}}{520469842636666622693081088000000} - \\ & \frac{\pi^{27} \omega^{27}}{1461479318123759876522171695104000000} + \\ & \frac{\pi^{29} \omega^{29}}{4746884825265972078944013665697792000000} - \\ & \frac{\pi^{31} \omega^{31}}{17658411549989416133671730836395786240000000} + \\ & \frac{\pi^{33} \omega^{33}}{74589130387155293748629391052935801077760000000} - \\ & \frac{\pi^{35} \omega^{35}}{355044260642859198243475901411974413130137600000000} + \\ & \frac{\pi^{37} \omega^{37}}{1891675820705153808241239602722999673157373132800000000} - \\ & \frac{\pi^{39} \omega^{39}}{11213854265140151775254068364941942062476907931238400000000}; \end{aligned}$$

```
Clear[determ];
```

```
determ[\omega] =
```

$$(\beta m^2 - 1) \text{tayS}[\omega]^4 + (1 + 2 \omega^2 (\alpha m - \beta m) \beta m) \text{tayS}[\omega]^2 + \omega^2 (\omega^2 (\alpha m - \beta m)^2 - \alpha m^2);$$

5. Find first eigenvalue:

```
FindRoot[determ[\omega] == 0, {\omega, .7, 0, 1}]
```

```
{\omega -> 0.995592}
```

6. Find higher order roots using Taylor series expansion:

```
taysol = Solve[determ[\omega] == 0, \omega];
```

```
L = Length[taysol];
```

```
roots = Table[\omega /. taysol[[i]], {i, 1, L}];
```

```
determRoots = Table[Abs[determ[\omega /. taysol[[i]]]], {i, 1, L}];
```

Filter out roots with an accuracy of less than 10⁻¹²:

```
p = Position[Round[Table[10^12 determRoots[[i]], {i, 1, L}], 0];
n = Length[p];
```

```
Table[determRoots[[p[[i]]]], {i, 1, n}];
```

Display all accurate roots:

```
Table[roots[[p[[i]]]], {i, 1, n}];
```

Display all position roots:

```
q = Table[roots[[p[[i]]]], {i, n - n/2, n}];
```

7. Check roots found from Taylor series expansion determinate equation with the determinate equation from Martin's paper:

```
Table[Abs[determin[q[[i]]]], {i, 1, Length[q]}];
```

8. Iterative process for greater accuracy of higher order roots:

NOTE: Define ω_1 as the leading eigenvalue. Redefine the variable 'determ' with 'determ1' on first iteration. Then, define ω_2 as the second eigenvalue and redefine 'determ1' with 'determ2' on second iteration, as so on.

1st iteration:

```
 $\omega_1 = 0.9955950186885631`;$ 
```

```
 $\text{determ1}[\omega_] = \frac{\text{determ}[\omega]}{\omega - \omega_1};$ 
```

2nd iteration:

```
 $\omega_2 = 1;$ 
```

```
 $\text{determ2}[\omega_] = \frac{\text{determ1}[\omega]}{(\omega - \omega_2)};$ 
```

3rd iteration:

```
 $\omega_3 = 1.973961228645531` - 0.15460532188869777` i;$ 
```

```
 $\text{determ3}[\omega_] = \frac{\text{determ2}[\omega]}{(\omega - \omega_3)};$ 
```

4th iteration:

MATHEMATICA PROGRAM FOR DETERMINING STRESS AND DISPLACEMENT EQUATIONS IN A BIMATERIAL

1. Solution for real roots:

Stress equations:

Constant relationships are found from boundary conditions. To determine these, run the Stress equation subset of commands, with out constant relationships, then set ψ equal to zero.

```
Clear[C1r, C2r, C3r, C4r,  $\psi$ , f,  $\phi$ ,  $\lambda$ ];

C4r = -C2r;
C3r = -C1r  $\frac{(\lambda + 1)}{(\lambda - 1)}$ ;

 $\phi = r^{(\lambda + 1)} * f$ ;
f = C1r * Sin[( $\lambda + 1$ ) *  $\psi$ ] +
  C2r * Cos[( $\lambda + 1$ ) *  $\psi$ ] + C3r * Sin[( $\lambda - 1$ ) *  $\psi$ ] + C4r * Cos[( $\lambda - 1$ ) *  $\psi$ ];

 $\sigma_{\theta\theta} = D[\phi, \{r, 2\}]$ ;
 $\sigma_{rr} = \frac{1}{r^2} * D[\phi, \{\psi, 2\}] + \frac{1}{r} * D[\phi, r]$ ;
 $\sigma_{r\theta} = \frac{1}{r^2} * (D[\phi, \psi]) - \frac{1}{r} * (D[\phi, r, \psi])$ ;
```

Strain equations (plane strain assumption):

$$v_1 = \frac{v}{1 - v};$$

$$E_1 = \frac{E_1}{1 - v^2};$$

$$e_{rr} = 1 / E_1 (\sigma_{rr} - v_1 * \sigma_{\theta\theta});$$

$$e_{\theta\theta} = 1 / E_1 (\sigma_{\theta\theta} - v_1 * \sigma_{rr});$$

Displacement equations:

$$u_{r1} = \int e_{rr} dr;$$

$$u_{\theta 1} = \int (r * e_{\theta\theta} - u_{r1}) d\psi;$$

Checking displacements:

$$\omega_4 = 2.942086864910637 - 0.32555258660879016 i;$$

$$\text{determ4}[\omega_] = \frac{\text{determ3}[\omega]}{(\omega - \omega_4)};$$

5th iteration:

$$\omega_5 = 3.924701634098341 - 0.4933398652658574 i;$$

$$\text{determ5}[\omega_] = \frac{\text{determ4}[\omega]}{(\omega - \omega_5)};$$

6th iteration:

$$\omega_6 = 4.9200942759197055 - 0.631068635356104 i;$$

$$\text{determ6}[\omega_] = \frac{\text{determ5}[\omega]}{(\omega - \omega_6)};$$

9. Display results:

Display roots:

$$\{\omega_1, \omega_2, \omega_3, \omega_4, \omega_5, \omega_6\}$$

$$\{0.995595, 1, 1.97396 - 0.154605 i,$$

$$2.94209 - 0.325553 i, 3.9247 - 0.49334 i, 4.92009 - 0.631069 i\}$$

Display accuracy of roots:

$$\{\text{Abs}[\text{determin}[\omega_1]], \text{Abs}[\text{determin}[\omega_2]], \text{Abs}[\text{determin}[\omega_3]],$$

$$\text{Abs}[\text{determin}[\omega_4]], \text{Abs}[\text{determin}[\omega_5]], \text{Abs}[\text{determin}[\omega_6]]\}$$

$$\{6.66134 \times 10^{-16}, 0., 2.79821 \times 10^{-16},$$

$$9.03656 \times 10^{-16}, 2.35514 \times 10^{-16}, 1.17839 \times 10^{-12}\}$$

$$G1 = \frac{E1}{2(1+\nu1)};$$

$$\gamma r \theta 1 = D[u \theta 1, r] + \frac{1}{r} * D[ur1, \psi] - \frac{u \theta 1}{r};$$

$$\gamma r \theta 2 = 2 * \frac{(1+\nu1)}{E1} * \sigma r \theta;$$

$$\text{Simplify}[\gamma r \theta 1 - \gamma r \theta 2];$$

$$\text{lam} = \mu * 2 \nu / (1 - 2 \nu);$$

$$\sigma r r 2 = (\text{lam} + 2 \mu) * D[ur1, r] + \text{lam} * \left(\frac{1}{r} D[u \theta 1, \psi] + \frac{ur1}{r} \right);$$

$$\sigma \theta \theta 2 = \text{lam} * D[ur1, r] + (\text{lam} + 2 \mu) * \left(\frac{1}{r} D[u \theta 1, \psi] + \frac{ur1}{r} \right);$$

$$\sigma r \theta 2 = \mu * \left(\frac{1}{r} D[ur1, \psi] + D[u \theta 1, r] - \frac{u \theta 1}{r} \right);$$

$$\text{Simplify}\left[D[\sigma r r 2, r] + \frac{1}{r} * D[\sigma r \theta 2, \psi] + \frac{\sigma r r 2 - \sigma \theta \theta 2}{r}\right];$$

$$\text{Simplify}\left[\frac{1}{r} * D[\sigma \theta \theta 2, \psi] + D[\sigma r \theta 2, r] + 2 * \frac{\sigma r \theta 2}{r}\right];$$

2. Solution for roots equal to one:

Stress equations:

Constant relationships are found from boundary conditions, determined as described in 'Solution for real roots' above.

$$\text{Clear}[C1r, C2r, C3r, C4r, \psi, f, \phi, \lambda];$$

$$C4r = -C2r;$$

$$C3r = -C1r - C1r * \lambda;$$

$$\lambda = 1;$$

$$\phi = r^{(\lambda+1)} * f;$$

$$f = C1r * \text{Sin}[(\lambda + 1) * \psi] + C2r * \text{Cos}[(\lambda + 1) * \psi] + C3r * \psi + C4r;$$

$$\sigma \theta \theta = D[\phi, \{r, 2\}];$$

$$\sigma r r = \frac{1}{r^2} * D[\phi, \{\psi, 2\}] + \frac{1}{r} * D[\phi, r];$$

$$\sigma r \theta = \frac{1}{r^2} * (D[\phi, \psi]) - \frac{1}{r} * (D[\phi, r, \psi]);$$

Checking the biharmonic eqn:

$$\phi2 = D[\phi, \{r, 2\}] + \frac{1}{r} * D[\phi, r] + \frac{1}{r^2} * (D[\phi, \{\psi, 2\}]);$$

$$\phi4 = D[\phi2, \{r, 2\}] + \frac{1}{r} * D[\phi2, r] + \frac{1}{r^2} * (D[\phi2, \{\psi, 2\}]);$$

$$q = \text{Simplify}[\phi4]$$

$$0$$

Strain equations (plane strain assumption):

$$v1 = \frac{\nu}{1 - \nu};$$

$$E1 = \frac{E11}{1 - \nu^2};$$

$$err = 1 / E1 (\sigma_{rr} - v1 * \sigma_{\theta\theta});$$

$$e_{\theta\theta} = 1 / E1 (\sigma_{\theta\theta} - v1 * \sigma_{rr});$$

Displacement equations:

$$ur1 = \int err \, dr + g1[\psi];$$

$$ur2 = \int err \, dr;$$

$$u_{\theta 1} = \int (r * e_{\theta\theta} - ur2) \, d\psi + g2[r] + \int g1[\psi] \, d\psi;$$

Checking displacements:

$$G1 = \frac{E1}{2 (1 + v1)};$$

$$\gamma_{r\theta 1} = D[u_{\theta 1}, r] + \frac{1}{r} * D[ur1, \psi] - \frac{u_{\theta 1}}{r};$$

$$\gamma_{r\theta 2} = 2 * \frac{(1 + v1)}{E1} * \sigma_{r\theta};$$

$$\text{Simplify}[\gamma_{r\theta 1} - \gamma_{r\theta 2}]$$

$$\frac{-8 C1 r r + 8 C1 r r v^2 - E11 g2[r] - E11 \int g1[\psi] \, d\psi + E11 g1'[\psi] + E11 r g2'[r]}{E11 r}$$

$$lam = \mu * 2 \nu / (1 - 2 \nu);$$

$$\begin{aligned} \sigma_{rr2} &= (1\text{am} + 2\ \mu) * D[\text{ur}1, r] + 1\text{am} * \left(\frac{1}{r} D[\text{u}\theta 1, \psi] + \frac{\text{ur}1}{r} \right); \\ \sigma_{\theta\theta 2} &= 1\text{am} * D[\text{ur}1, r] + (1\text{am} + 2\ \mu) * \left(\frac{1}{r} D[\text{u}\theta 1, \psi] + \frac{\text{ur}1}{r} \right); \\ \sigma_{r\theta 2} &= \mu * \left(\frac{1}{r} D[\text{ur}1, \psi] + D[\text{u}\theta 1, r] - \frac{\text{u}\theta 1}{r} \right); \\ \text{Simplify}\left[D[\sigma_{rr2}, r] + \frac{1}{r} * D[\sigma_{r\theta 2}, \psi] + \frac{\sigma_{rr2} - \sigma_{\theta\theta 2}}{r} \right] \\ \text{Simplify}\left[\frac{1}{r} * D[\sigma_{\theta\theta 2}, \psi] + D[\sigma_{r\theta 2}, r] + 2 * \frac{\sigma_{r\theta 2}}{r} \right] \\ &= \frac{\mu \left((-5 + 6\ \nu) g_1[\psi] + (1 - 2\ \nu) g_1''[\psi] \right)}{r^2 (-1 + 2\ \nu)} \\ &= \frac{1}{E_{11} r^2 (-1 + 2\ \nu)} \\ & \left(\mu \left(16 C_{1r} r - 32 C_{1r} r \nu - 16 C_{1r} r \nu^2 + 32 C_{1r} r \nu^3 + (E_{11} - 2 E_{11} \nu) g_2[r] + \right. \right. \\ & \quad \left. \left. (E_{11} - 2 E_{11} \nu) \int g_1[\psi] d\psi - 5 E_{11} g_1'[\psi] + 6 E_{11} \nu g_1'[\psi] - \right. \right. \\ & \quad \left. \left. E_{11} r g_2'[r] + 2 E_{11} r \nu g_2'[r] - E_{11} r^2 g_2''[r] + 2 E_{11} r^2 \nu g_2''[r] \right) \right) \end{aligned}$$

Looking closer at $g_2[r]$:

Using θ instead of ψ in calculations below.

$$\begin{aligned} \sigma_{rr} &= -2 (C_{2r} + 2 C_{1r} \theta + C_{2r} \cos[2\ \theta] + C_{1r} \sin[2\ \theta]); \\ \sigma_{\theta\theta} &= 2 (-C_{2r} - 2 C_{1r} \theta + C_{2r} \cos[2\ \theta] + C_{1r} \sin[2\ \theta]); \\ \sigma_{r\theta} &= 4 \sin[\theta] (C_{2r} \cos[\theta] + C_{1r} \sin[\theta]); \\ \text{Clear}[C_{1r}, C_{2r}, C_{3r}, C_{4r}, \psi, f, \phi, \lambda, \theta, L, g_2, g_1]; \\ \text{errS} &= \text{Simplify}\left[\frac{1}{e_1} * (\sigma_{rr} - \nu * \sigma_{\theta\theta}) \right]; \\ \text{ur} &= \int \text{errS} dr + g_1[\theta]; \\ \epsilon_{\theta\theta S} &= \text{errS}; \\ \text{u}\theta &= \int (r * \epsilon_{\theta\theta S} - \text{ur}) d\theta + g_2[r]; \end{aligned}$$

$$\begin{aligned}
 G &= \frac{e1}{2(1+\nu)}; \\
 \gamma r \theta S &= \frac{1}{G} * c r \theta; \\
 \gamma r \theta D &= D[u\theta, r] + \frac{1}{r} * D[ur, \theta] - \frac{u\theta}{r}; \\
 zero1 &= \text{Simplify}[\gamma r \theta S - \gamma r \theta D] \\
 &= \frac{-8 C1 r r - e1 g2[r] + e1 \int g1[\theta] d\theta + e1 g1'[\theta] + e1 r g2'[r]}{e1 r}
 \end{aligned}$$

Isolate r-dependence terms:

$$\begin{aligned}
 zero2 &= -8 C1 r r - e1 g2[r] + e1 r g2'[r] \\
 &= -8 C1 r r - e1 g2[r] + e1 r g2'[r]
 \end{aligned}$$

Solve differential equation with constant of integration:

$$\begin{aligned}
 int &= \text{Exp}\left[\int \frac{-1}{r} dr\right]; \\
 g2[x_] &= \left(\int \frac{8 C1}{e1} * int dr + L\right) / int
 \end{aligned}$$

3. Solution for complex roots:

Stress equations:

Constant relationships are found from boundary conditions, determined of these and formulation of stress function is found in appendix title "MATHEMATICA PROGRAM FOR DETERMINING THE STRESS FUNCTION FOR COMPLEX ROOTS"

$$\begin{aligned}
 \phi C &= \frac{1}{\eta^2 + (-1 + \xi)^2} \\
 &= \frac{4 r^{1+\xi} (\text{Cosh}[\eta \psi] ((A1 (\beta \eta + \alpha (\eta^2 + (-1 + \xi) \xi)) + A2 (\alpha \eta - \beta (\eta^2 + (-1 + \xi) \xi))) \\
 &\quad \text{Cos}[\xi \psi] \text{Sin}[\psi] - ((A1 (\beta \eta + \alpha (-1 + \xi)) + A2 (\beta + \alpha \eta - \beta \xi)) \text{Cos}[\psi] + \\
 &\quad (B1 \alpha - B2 \beta) (\eta^2 + (-1 + \xi)^2) \text{Sin}[\psi]) \text{Sin}[\xi \psi]) + \\
 &\quad ((A2 (\beta \eta + \alpha (-1 + \xi)) - A1 (\beta + \alpha \eta - \beta \xi)) \text{Cos}[\psi] \text{Cos}[\xi \psi] + \text{Sin}[\psi] \\
 &\quad ((B2 \alpha + B1 \beta) (\eta^2 + (-1 + \xi)^2) \text{Cos}[\xi \psi] + (A2 (\beta \eta + \alpha (\eta^2 + (-1 + \xi) \xi)) + \\
 &\quad A1 (-\alpha \eta + \beta (\eta^2 + (-1 + \xi) \xi))) \text{Sin}[\xi \psi])) \text{Sinh}[\eta \psi])}{\eta^2 + (-1 + \xi)^2} \\
 \alpha &= \text{Cos}[\eta * \text{Log}[r]]; \\
 \beta &= \text{Sin}[\eta * \text{Log}[r]];
 \end{aligned}$$

$$\begin{aligned}\sigma_{\theta\theta C} &= D[\phi C, \{r, 2\}]; \\ \sigma_{rr C} &= \frac{1}{r^2} * D[\phi C, \{\psi, 2\}] + \frac{1}{r} * D[\phi C, r]; \\ \sigma_{r\theta C} &= \frac{1}{r^2} * (D[\phi C, \psi]) - \frac{1}{r} * (D[\phi C, r, \psi]);\end{aligned}$$

Strain equations (plane strain assumption):

$$\begin{aligned}v_1 &= \frac{\nu}{1 - \nu}; \\ E_1 &= \frac{E_1}{1 - \nu^2}; \\ \epsilon_{rr C} &= 1 / E_1 (\sigma_{rr C} - \nu_1 * \sigma_{\theta\theta C}); \\ \epsilon_{\theta\theta C} &= 1 / E_1 (\sigma_{\theta\theta C} - \nu_1 * \sigma_{rr C});\end{aligned}$$

Displacement equations:

$$\begin{aligned}u_r C &= \text{Simplify}[\int \epsilon_{rr C} dr]; \\ u_{\theta C} &= \text{Simplify}[\int (r * \epsilon_{\theta\theta C} - u_r) d\psi];\end{aligned}$$

MATHEMATICA PROGRAM FOR DETERMINING THE STRESS FUNCTION FOR COMPLEX ROOTS

Define constants in terms of complex parts:

```

Clear[ψ]

Ac = (A1 + i * A2);
Bc = (B1 + i * B2);
Cc = (C1 + i * C2);
Dc = (D1 + i * D2);
Acbar = (A1 - i * A2);
Bcbar = (B1 - i * B2);
Ccbar = (C1 - i * C2);
Dcbar = (D1 - i * D2);

```

Apply known boundary conditions from real case:

```

Dc = -Bc;
Cc = -Ac * (λ + 1) / (λ - 1);
Dcbar = -Bcbar;
Ccbar = -Acbar * (λbar + 1) / (λbar - 1);

```

Define stress function in terms of complex constants and eigenvalue:

```

φ1 = rλ+1 * (
    Ac * Sin[(λ + 1) * ψ] +
    Bc * Cos[(λ + 1) * ψ] +
    Cc * Sin[(λ - 1) * ψ] +
    Dc * Cos[(λ - 1) * ψ]
);

φ2 = φ1 / . λ -> (ξ + i * η);

φ3 = r1+ξ * (α + i * β) *
    ( (-B1 - i B2) Cos[(-1 + i η + ξ) ψ] + (B1 + i B2) Cos[(1 + i η + ξ) ψ] +
      (-A1 - i A2) (1 + i η + ξ) Sin[(-1 + i η + ξ) ψ] /
      (-1 + i η + ξ) +
      (A1 + i A2) Sin[(1 + i η + ξ) ψ] );

φ4 = Expand[φ3];

```

Define stress function in terms of complex conjugate constants and eigenvalue:

```


$$\phi_{1c} = r^{\lambda_{bar}+1} * ($$


$$Acbar * Sin[(\lambda_{bar} + 1) * \psi] +$$


$$Bcbar * Cos[(\lambda_{bar} + 1) * \psi] +$$


$$Ccbar * Sin[(\lambda_{bar} - 1) * \psi] +$$


$$Dcbar * Cos[(\lambda_{bar} - 1) * \psi]$$


$$);$$


$$\phi_{2c} = \phi_{1c} / . \lambda_{bar} \rightarrow (\xi - i * \eta);$$


$$\phi_{3c} = (\alpha - i * \beta) * r^{\xi+1} *$$


$$\left( (-B1 + i B2) Cos[(-1 - i \eta + \xi) \psi] + (B1 - i B2) Cos[(1 - i \eta + \xi) \psi] + \right.$$


$$\frac{(-A1 + i A2) (1 - i \eta + \xi) Sin[(-1 - i \eta + \xi) \psi]}{-1 - i \eta + \xi} +$$


$$\left. (A1 - i A2) Sin[(1 - i \eta + \xi) \psi] \right);$$


$$\phi_{4c} = Expand[\phi_{3c}];$$


```

Define stress function as a sum of the complex conjugate stress functions:

```


$$\phi_{tot1} = \phi_4 + \phi_{4c};$$


$$\phi_{tot2} = Simplify[\phi_{tot1}];$$


```

Check biharmonic equation:

```

Clear[\psi]

$$\phi = \phi_C;$$


$$\phi_{2ch} = D[\phi, \{r, 2\}] + \frac{1}{r} * D[\phi, r] + \frac{1}{r^2} * (D[\phi, \{\psi, 2\}]);$$


$$\phi_{4ch} = D[\phi_{2ch}, \{r, 2\}] + \frac{1}{r} * D[\phi_{2ch}, r] + \frac{1}{r^2} * (D[\phi_{2ch}, \{\psi, 2\}]);$$


$$q = Simplify[\phi_{4ch}]$$

0

```

MATHEMATICA PROGRAM FOR DETERMINING THE STRESS INTENSITY FACTOR AND SINGULARITY DOMINATED ZONE

1. Set directory, read in file, and define normalization constant:

NOTE: Must first have text file with raw data

```
Clear[r,  $\theta$ ]  
  
<< Graphics`Graphics`  
  
w = 10 * 10^5;  
  
Directory[];  
  
SetDirectory["C:\\folder name"];  
  
xposf = ReadList["x1.txt"];  
ypos = ReadList["y1.txt"] / w;  
oxdat = ReadList["x stress.txt"];  
oydat = ReadList["y stress.txt"];  
txydat = ReadList["xy stress.txt"];  
  
L = Length[xposf];
```

Adjust x displacement:

```
xpos = (xposf + 50) / w;
```

2. Convert cartesian data to polar coordinates:

```

rdat = Table[(xpos[[i]]2 + ypos[[i]]2).5, {i, 1, L}];
θdat = Table[ArcTan[xpos[[i]], ypos[[i]]], {i, 1, L}];

ordat = Table[Sin[θdat[[i]]] *
  (rxydat[[i]] * Cos[θdat[[i]]] + oydat[[i]] * Sin[θdat[[i]]) +
  Cos[θdat[[i]]] * (oxdat[[i]] * Cos[θdat[[i]]] +
  rxydat[[i]] * Sin[θdat[[i]]]), {i, 1, L}];

rrθdat = Table[Cos[θdat[[i]]] *
  (rxydat[[i]] * Cos[θdat[[i]]] + oydat[[i]] * Sin[θdat[[i]]) -
  Sin[θdat[[i]]] * (oxdat[[i]] * Cos[θdat[[i]]] +
  rxydat[[i]] * Sin[θdat[[i]]]), {i, 1, L}];

rθrdat = Table[Cos[θdat[[i]]] *
  (rxydat[[i]] * Cos[θdat[[i]]] - oxdat[[i]] * Sin[θdat[[i]]) +
  Sin[θdat[[i]]] * (oydat[[i]] * Cos[θdat[[i]]] -
  rxydat[[i]] * Sin[θdat[[i]]]), {i, 1, L}];

oθdat = Table[-Sin[θdat[[i]]] *
  (rxydat[[i]] * Cos[θdat[[i]]] - oxdat[[i]] * Sin[θdat[[i]]) +
  Cos[θdat[[i]]] * (oydat[[i]] * Cos[θdat[[i]]] -
  rxydat[[i]] * Sin[θdat[[i]]]), {i, 1, L}];

```

NOTE: θ and ψ are measured in radians

3. Isolate data in a specified region:

User defined number of terms in model to collocate and desired redundancy (if variable 'int' is less than one, user must increase either variable 'NumTerm' or 'red')

```

NumTerm = 20;
red = 19.;
r1 = 4.5 / w;
ptsdes = red * NumTerm;
zone1a = {};
zone1 = {};
Chop[Table[If[rdat[[i]] < r1, AppendTo[zone1a, i]], {i, 1, L}]];
L1a = Length[zone1a];
int =  $\frac{L1a}{ptsdes}$ 
int1 = Ceiling[int];
zone1 = Table[zone1a[[Ceiling[int * i] - int1 + 1]], {i, 1, ptsdes}];
L1 = Length[zone1];

```

Isolate stress and locations in desired region:

```

r1dat = rdat[[zone1]];
θ1dat = θdat[[zone1]];

x1pos = xpos[[zone1]];
y1pos = ypos[[zone1]];
σr1dat = σrdat[[zone1]];

line1 = Table[{x1pos[[i]], y1pos[[i]]}, {i, 1, Length[zone1]};

```

Plot specified region

```
ListPlot[line1, PlotStyle -> PointSize[.01], PlotRange -> All];
```

4. Define radial stress equation:

Set eigenvalues and constants:

```

λ = {0.9955950186885631`, 1, 1.973961228645531` - 0.15460532188869777` i,
      1.973961228645531` + 0.15460532188869777` i,
      2.942086864910637` - 0.32555258660879016` i,
      2.942086864910637` + 0.32555258660879016` i,
      3.924701634098341` - 0.4933398652658574` i,
      3.924701634098341` + 0.4933398652658574` i,
      4.9200942759197055` - 0.631068635356104` i,
      4.9200942759197055` + 0.631068635356104` i};

l = Length[λ] - 4;

```

NOTE: The sub i is the λ number, so $C3C_4$ is the fourth λ , the C means its complex, the $C3$ refers to $B1$ from the original stress function.

```

η = Table[Im[λ[[i + 2 - 2]]], {i, 3, l}]
δr = Table[Re[λ[[i]]], {i, 1, l}]
ξ = Table[Re[λ[[i + 2 - 2]]], {i, 3, l}]
C1r = Table[C1Ri, {i, 1, l}];
C2r = Table[C2Ri, {i, 1, l}];
C1o = Table[C1Ri, {i, 2, 2}];
C2o = Table[C2Ri, {i, 2, 2}];
A1 = Table[C1Ci, {i, 3, l}]
A2 = Table[C2Ci, {i, 3, l}]
B1 = Table[C3Ci, {i, 3, l}]
B2 = Table[C4Ci, {i, 3, l}]

```

Real root stress (τ_{rrreal}):

```
Clear[r, \theta, \tau r \theta basic, \tau \theta \theta basic, \tau r \theta sum, \tau \theta \theta sum, \psi]

\tau r r real = \frac{1}{-1 + \delta r}
(2 r^{-1 + \delta r} \delta r (\text{Sin}[\psi] (-C1r (-2 - \delta r + \delta r^2) \text{Cos}[\delta r \psi] + C2r (-1 + \delta r)^2 \text{Sin}[\delta r \psi]) -
\text{Cos}[\psi] (2 C2r (-1 + \delta r) \text{Cos}[\delta r \psi] + C1r (1 + \delta r) \text{Sin}[\delta r \psi]))) ;
Collect[\tau r r real, {C1R1, C2R1}];
```

Unity root stress (τ_{rrreal}):

```
\tau r r real1 = -2 (C2o + 2 C1o \psi + C2o \text{Cos}[2 \psi] + C1o \text{Sin}[2 \psi]);
```

Complex root stress ($\tau_{rrcomplex}$):

```
\tau r r complex = \frac{1}{\eta^2 + (-1 + \xi)^2}
(4 r^{-1 + \xi} (\text{Cosh}[\eta \psi] (\text{Cos}[\psi] (2 (\eta^2 + (-1 + \xi)^2) \text{Cos}[\xi \psi] ((B2 \eta - B1 \xi)
\text{Cos}[\eta \text{Log}[r]] + (B1 \eta + B2 \xi) \text{Sin}[\eta \text{Log}[r]])) +
\text{Sin}[\xi \psi] ((A2 \eta (-1 + \eta^2 - 2 \xi + \xi^2) - A1 (\eta^2 (2 + \xi) + \xi (-1 + \xi^2)))
\text{Cos}[\eta \text{Log}[r]] + (A1 \eta (-1 + \eta^2 - 2 \xi + \xi^2) +
A2 (\eta^2 (2 + \xi) + \xi (-1 + \xi^2))) \text{Sin}[\eta \text{Log}[r]])) +
\text{Sin}[\psi] ((\eta^2 + (-1 + \xi)^2) \text{Sin}[\xi \psi] ((B2 (\eta - 2 \eta \xi) - B1 (\eta^2 + \xi - \xi^2))
\text{Cos}[\eta \text{Log}[r]] + (B1 (\eta - 2 \eta \xi) + B2 (\eta^2 + \xi - \xi^2))
\text{Sin}[\eta \text{Log}[r]])) + \text{Cos}[\xi \psi] ((2 A2 \eta (1 + \xi + \eta^2 \xi - 2 \xi^2 + \xi^3) +
A1 (\eta^4 + \eta^2 (3 - 2 \xi) + \xi (-2 + \xi + 2 \xi^2 - \xi^3)))
\text{Cos}[\eta \text{Log}[r]] + (2 A1 \eta (1 + \xi + \eta^2 \xi - 2 \xi^2 + \xi^3) - A2
(\eta^4 + \eta^2 (3 - 2 \xi) + \xi (-2 + \xi + 2 \xi^2 - \xi^3))) \text{Sin}[\eta \text{Log}[r]])) +
(\text{Cos}[\psi] (-2 (\eta^2 + (-1 + \xi)^2) \text{Sin}[\xi \psi] ((B1 \eta + B2 \xi) \text{Cos}[\eta \text{Log}[r]] +
(-B2 \eta + B1 \xi) \text{Sin}[\eta \text{Log}[r]])) +
\text{Cos}[\xi \psi] ((A1 \eta (-1 + \eta^2 - 2 \xi + \xi^2) + A2 (\eta^2 (2 + \xi) + \xi (-1 + \xi^2)))
\text{Cos}[\eta \text{Log}[r]] + (-A2 \eta (-1 + \eta^2 - 2 \xi + \xi^2) +
A1 (\eta^2 (2 + \xi) + \xi (-1 + \xi^2))) \text{Sin}[\eta \text{Log}[r]])) +
\text{Sin}[\psi] ((\eta^2 + (-1 + \xi)^2) \text{Cos}[\xi \psi] ((B1 (\eta - 2 \eta \xi) + B2 (\eta^2 + \xi - \xi^2))
\text{Cos}[\eta \text{Log}[r]] + (B2 \eta (-1 + 2 \xi) + B1 (\eta^2 + \xi - \xi^2))
\text{Sin}[\eta \text{Log}[r]])) + \text{Sin}[\xi \psi] ((-2 A1 \eta (1 + \xi + \eta^2 \xi - 2 \xi^2 + \xi^3) +
A2 (\eta^4 + \eta^2 (3 - 2 \xi) + \xi (-2 + \xi + 2 \xi^2 - \xi^3))) \text{Cos}[\eta \text{Log}[r]] +
(2 A2 \eta (1 + \xi + \eta^2 \xi - 2 \xi^2 + \xi^3) + A1 (\eta^4 + \eta^2 (3 - 2 \xi) +
\xi (-2 + \xi + 2 \xi^2 - \xi^3))) \text{Sin}[\eta \text{Log}[r]])) \text{Sinh}[\eta \psi]));

\tau r r complex1 = \text{Sum}[\tau r r complex[[i]], {i, 1, 4}];
```

Sum stress cases for full parameter model:

```

trrsum1 = trrreal[[1]] + trrreal1[[1]] + trrcomplex1;
trrsum = trrsum1 /.  $\psi \rightarrow \theta - \pi / 2$ ;

```

5. Collocate data with stress equation:

NOTE: To find stress intensity, several iterations must be run. First input model data into step 3. Then, collocate different the appropriate list, noting the 1st two leading terms. Repeat for all the different parameter models.

Set up local collocation scheme (nonlinear fit will give a warning when convergence of a coefficient is reached):

```

<< Statistics`NonlinearFit`
<< Statistics`Common`PopulationsCommon`

```

Define variable 'data' as the data in the specified region:

```

data = Table[{r1dat[[i]],  $\theta$ 1dat[[i]],  $\sigma$ r1dat[[i]]}, {i, 1, L1}];
rhs = trrsum;

```

List comands are for convience to input into fitting function:

```

list2 = {C1R1, C2R1};
list4 = {C1R1, C2R1, C1R2, C2R2,};
list8 = {C1R1, C2R1, C1R2, C2R2, C1C3, C2C3, C3C3, C4C3};
list12 =
  {C1R1, C2R1, C1R2, C2R2, C1C3, C2C3, C3C3, C4C3, C1C4, C2C4, C3C4, C4C4};
list16 = {C1R1, C2R1, C1R2, C2R2, C1C3, C2C3, C3C3, C4C3,
  C1C4, C2C4, C3C4, C4C4, C1C5, C2C5, C3C5, C4C5};
list20 = {C1R1, C2R1, C1R2, C2R2, C1C3, C2C3, C3C3, C4C3, C1C4, C2C4,
  C3C4, C4C4, C1C5, C2C5, C3C5, C4C5, C1C6, C2C6, C3C6, C4C6};

sol = NonlinearRegress[data, rhs, {r,  $\theta$ }, list20];
par = BestFitParameters /. sol[[1]]

```

6. Calculation of relative error:

$$\frac{1}{L1} \left(\text{Sum} \left[\left(\frac{1}{\sigma r1dat[[i]]} (\sigma r1dat[[i]] - rhs16 /. \{r \rightarrow data[[i]][[1]], \theta \rightarrow data[[i]][[2]]\} /. par16) \right)^2, \{i, 1, L1\} \right] \right)^{.5 * 100};$$

7. Graphical comparison of fitted function:

Define angular orientation comparison, comparison will take place along a radial line for a given θ value, default set to $\theta = 0$ (w is the width in which data can be taken to capture more data points):

```

 $\theta_{ch} = \text{ArcTan}[\text{xpos}[[30]] / \text{ypos}[[600]]];$ 
 $\theta_{ch} = 0;$ 
 $w = 0.00;$ 
 $\text{zone0} = {};$ 
 $\theta_{ch1} = \theta_{ch} + w;$ 
 $\theta_{ch2} = \theta_{ch} - w;$ 
Chop[Table[If[ $\theta_{dat}[[i]] \leq \theta_{ch1}$  &&  $\theta_{dat}[[i]] \geq \theta_{ch2}$  &&  $\text{rdat}[[i]] < r1$ ,
  AppendTo[zone0, i]], {i, 1, L}]];
 $\text{rdat0} = \text{rdat}[[\text{zone0}]];$ 
 $\text{xpos0} = \text{xpos}[[\text{zone0}]];$ 
 $\text{ypos0} = \text{ypos}[[\text{zone0}]];$ 
 $\text{ordat0} = \text{ordat}[[\text{zone0}]];$ 
 $\theta_{dat0} = \theta_{dat}[[\text{zone0}]];$ 

```

Plot data points

```

pts = Table[{xpos0[[i]], ypos0[[i]]}, {i, 1, Length[zone0]};
ListPlot[pts, PlotStyle -> PointSize[.02], PlotRange -> {{0, r1}, {0, r1}}]

```

Plot discretize model into data points:

```

discmod = Table[
  rhs /. {r -> rdat0[[i]],  $\theta$  ->  $\theta_{dat0}[[i]]$ } /. par, {i, 1, Length[zone0]};
dmod = Table[{rdat0[[i]], discmod[[i]]}, {i, 1, Length[zone0]};
modpts = ListPlot[dmod,
  PlotStyle -> PointSize[.02], PlotRange -> {{0, r1}, {-1000, 800}}];

```

Plot model along given angular orientation:

```

 $\text{ormod0} = \text{rhs} /. \text{par};$ 
 $\theta = \theta_{ch};$ 
mod = Plot[ormod0, {r, 0, r1}, PlotRange -> {{0, r1}, {-1000, 800}}];

line0 = Table[{rdat0[[i]], ordat0[[i]]}, {i, 1, Length[zone0]};
points = ListPlot[line0,
  PlotStyle -> PointSize[.02], PlotRange -> {{0, r1}, {-1000, 800}}]

```

Show plots together for graphical comparison:

```

Show[{modpts16, mod16}];

Show[{points, mod16}, Frame -> True, GridLines -> Automatic];

```

```
Clear[y, n,  $\theta$ , r, x, w]
```

8. Determination of Singularity Dominated Zone

NOTE: To find SDZ, several iteration must be run. First input a value for θ from 0 to $\pi/2$. Then, check accuracy of solution with variable 'zero1' equal to zero. If not equal to zero adjust 'FindRoot' parameters. When equal to zero, note the value and continue process for different θ values.

```
Clear[r,  $\theta$ ]
```

```
 $\theta = 0 * \pi / 12;$ 
```

```
 $\sigma_{mod1} = \text{rrreal}[[1]] /. \{\psi \rightarrow \theta - \pi / 2,$ 
```

```
  C1R1 → "enter converged value", C2R1 → "enter converged value";
```

```
 $\sigma_{mod20} = \sigma_{mod0} = \text{rhs} /. \text{par};$ 
```

```
relE = Abs[ $\frac{(\sigma_{mod20} - \sigma_{mod1})}{\sigma_{mod20}}$ ] * 100;
```

```
qw = FindRoot[relE == 5, {r, {r1 / 10000, r1 / 100}}]
```

```
zero1 = relE /. qw[[1]]
```

Plot of relative error:

```
Plot[relE, {r, -r1 / 5000, r1 / 500},
```

```
  Frame → True, GridLines → Automatic, FrameLabel →
```

```
  {Radius (r - W), Relative Error (percent), Relative Error Plot, ""}]
```